Lappeenranta University of Technology
Faculty of Technology
Department of Energy and Environmental Technology

Droplet Deposition in the Last Stage of Steam Turbine

Supervisor: Teemu Turunen-Saaresti
Examiners: Teemu Turunen-Saaresti
Aki Grönman

Bidesh Sengupta
Punkkerikatu 5 C 49
53580 Lappeenranta
Finland
Tel: +358413697940

ABSTRACT

Lappeenranta University of Technology
Faculty of Technology
Department of Energy and Environmental Technology

Bidesh Sengupta
Droplet Deposition in the Last Stages of Steam Turbine
Master's Thesis
2016
58 pages, 33 figures, 3 tables and 3 appendixes

Examiners: Teemu Turunen-Saaresti
Aki Grönman

During the expansion of steam in turbine, the steam crosses the saturation line and hence subsequent turbine stages run under wet condition. The stages under wet condition run with low efficiency as compared to stages running with supersaturated steam and the life of the last stage cascade is reduced due to erosion. After the steam crosses the saturation line it does not condense immediately but instead it becomes supersaturated which is a meta-stable state and reversion of equilibrium results in the formation of large number of small droplets in the range of 0.05 - 1 μm. Although these droplets are small enough to follow the stream lines of vapor however some of the fog droplets are deposited on the blade surface. After deposition they coagulate into films and rivulets which are then drawn towards the trailing edge of the blade due to viscous drag of the steam. These large droplets in the range of radius 100 μm are accelerated by steam until they impact on the next blade row causing erosion. The two phenomenon responsible for deposition are inertial impaction and turbulent-diffusion. This work shall discuss the deposition mechanism in steam turbine in detail and numerically model and validate with practical data.

Table of Contents

Nomenclature

A	Area
C_g	Rate of Acquiring Molecule in a Droplet
C_p	Specific heat at constant pressure
C_v	Specific heat at constant volume
C_∞	Volumetric Concentration of Droplets outside Boundary Layer
D	Diffusion Coefficient of Droplets
$\boldsymbol{D}$	Drag Force
E	Total Energy
E_{g+1}, E_g	Evaporation Rate
$erfc$	Complementary Error Function
G	Gibb's Free Energy
$g - mer$	g number of molecules in a liquid droplet of radius r
h	Enthalpy
I	Nucleation Rate
I_g	Net growth Rate of a Droplet
Kn	Knudsen Number
k_s	Sand Grain Roughness Height
l_g	Mean Free Path of Vapor Molecule
m	Mass of Each Molecule
N	Mass Transfer Rate of Droplets to the Surface
n	Size Distribution of Droplets
P	Pressure
q	Heat Flux
q_c, q_e	Condensation and Evaporation Coefficient
R	Universal Gas Constant
$\boldsymbol{R}$	Position Vector
Re	Reynolds's Number
r	Radius of Mono dispersed Droplets
S	Saturation Ratio
Sc	Schmidt Number
s	Entropy
s'	Stop Distance
T	Temperature
u	Velocity along X direction
u_τ	Friction Velocity
u^+	Dimensionless Friction Velocity
V	Deposition Velocity of Droplets
$\boldsymbol{V}$	Vector form of Velocity
V_+	Dimensionless Deposition Velocity of Droplets
v	Velocity along Y direction
w	Velocity along Z direction
y	Distance from the Wall
y^+	Dimensionless Wall Coordinate

i, j, k	Unit Vectors
β	Wetness Fraction
γ	Specific Heat Ratio
Γ	Mass Generation per Unit Volume
ϵ	Eddy Diffusivity
η	Number of Droplets per Unit Volume
η^*	Ratio of droplet to gas RMS fluctuating velocity normal to the surface
θ	Angle in Cylindrical Coordinate
κ	Von Karman Constant
μ	Dynamic Viscosity
ν	Kinematic Viscosity of the Fluid
ρ	Fluid Density
σ	Liquid Surface Tension
τ	Stress Tensor
τ_r	Inertial Relaxation Time
τ_w	Wall Shear Stress
τ_+	Dimensionless Inertial Relaxation Time of the Droplets
υ	RMS Fluctuating Velocity Normal to the Surface
ω	Vorticity
$\boldsymbol{\Omega}$	Angular Velocity of the Turbine
∇	Del

Subscripts:

l	Droplet
g	Vapor
$*$	Critical
s	Saturation Condition
x, y, z	Coordinate axis

List of Acronyms

LP	Low Pressure
VS	Viscous Sublayer
BL	Buffer Layer
LL	Log Layer
TPDR	Turbulent Particle-Diffusion Regime
EDIR	Eddy-Diffusion Impaction Regime
PIMR	Particle Inertia-Moderated Regime

List of Figures

List of Tables

Acknowledgement

I am grateful to Associate Professor Teemu Turunen-Saaresti who is my supervisor. His deserves my greatest gratitude for his continuous support, guidance and faith on me.

I would like to thank all members of laboratory of fluid dynamics of Lappeenranta University of Technology, especially Alireza Ameli. I am thankful to Associate Professor Ahti Jaatinen-Värri, Associate Professor Aki Grönman and Jonna Tiainen for having enormous help in understanding the concept of turbomachinery better.

I am thankful to Dr. Ashvinkumar Chaudhari for his help and useful advice in several stages of my thesis.

The thesis would not be possible without the encouragement and motivation of my parent and friends. I am thankful to them.

1 Introduction

Erosion of rotor blades in steam turbine marks its history perhaps from its discovery due to wet steam flow at the last stages. Although, reviewing of the past literature suggests that there had been historically three stages that can be identified for the study of fog droplet deposition in steam turbine. In the first phase during 1960s and 1970s greater efforts were put to increase the capacity of steam turbine from existing 200MW to about 600 MW. Large turbine blades of one meter were introduced resulting high tip speed erosion and deposition on blades. This led to the study of predicting models for deposition with experimental set up such as deposition of air particle flow which were used to simulate the steam flow. But the theoretical estimates did not match quite well with experiments as the experimental results were large as compared to theory. Then during 1980s, ground breaking developments in optical instruments allowed more accurate measurements for fog droplet size distribution and improved probes enabled to measure the flow rate. This was during this period when steam turbine started to be standardized.

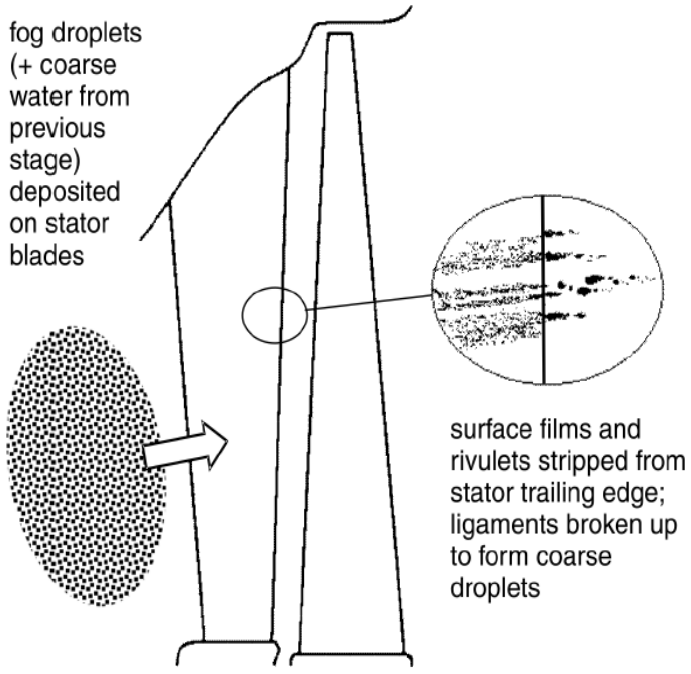

Figure 1: Schematic diagram of fog to coarse water droplet conversion process **[1]**

In the second phase, during 1990s gas turbine combined power plant dominated the power market. During this time steam turbines were improving quite slowly. Developers were mainly focusing on the aerodynamic design of the blade and efficiency achieved were quite high compared to earlier design and

therefore not much research and study on deposition were conducted during this period. It was during early twenty first century, namely the third phase when the requirement for power plant upgrading and retrofitting with supercritical steam and with the introduction of ultra-supercritical power plant where turbine has to operate in wet steam the study on deposition once again became necessary.

During second phase of development, mostly the experimental results were utilized to predict the behavior of wet steam inside turbine as computational results were not so reliable in early days for such complicated case. Therefore accurate prediction of deposition was rather difficult. During off design operation of steam turbine the problem seemed to be even vigorous. Sub-micron sized fog droplets (0.03 μm < r < 1 μm) are nucleated from the rapidly expanding steam and are deposited at the ultimate and penultimate stator blades. These droplets coagulates and forms rivulets which are broken down by strong aerodynamic forces into secondary or coarse droplets (10 μm < r < 100 μm). The droplets are then dragged towards the trailing edge of the stator blade due to viscous drag of the flowing steam which ultimately hits the rotor with high tip speed leading edge and cause erosion.

The droplet sizes has strong influence on the phenomenon of deposition on the turbine blades. The two mechanism responsible for deposition are turbulent diffusion and inertial impaction. Additional phenomenon that was discovered recently to be responsible for deposition is Thermophoresis. It shall be described in brief. The deposition of fog droplets in the last stages of LP steam turbine is the combination of turbulent diffusion as well as inertial impaction.

Many studies have been performed regarding the droplet nucleation and growth in nozzles and turbine cascade. The study on turbine cascade were extensively carried out both numerically and experimentally by Bhaktar et al. **[2, 3]** and White et al. **[4]**. Due to the complex flow behavior in turbine cascade, extensive 2D studies with numerical approach which was based on the inviscid time marching scheme with Lagrangian tracking by White and Young **[5]**, Bhaktar et al. **[6]** are noteworthy. Some works based on Eulerian-Eulerian multiphase method for condensing steam flows by Gerber and Kermani **[7],** Senoo and Shikano **[8]**. Recently notable work on the effect of droplet size on deposition and effect of interphase friction in a low pressure turbine cascade for last stage stator blade was presented by Starzmann et al. **[9]**. The results of the work found to be quite satisfactory and matches well with experiments. In contrast a little work regarding droplet deposition is performed for steam turbine. Although a large number of investigations were carried for diffusional deposition of small particles in turbulent flow pipes such as experimental study by Friedlander and Johnstone **[10]** on the rate of deposition of dust based on transport of particles in a turbulent stream, the work of Montgomery and Corn **[11]** on deposition in large pipes in

a complete turbulent flow of high Reynolds number. The experimental investigation of Benjamin et al. **[12]** on monodispersed particle deposition for wide range of particle size and dimensionless relaxation time is also noteworthy. The extensive mathematical works by Cleaver and Yates **[13]** for deposition of particles by diffusion in sub-layer and the paper of Reeks and Skyrme **[14]** illustrates that with the increase in particle size, the deposition is controlled by diffusional as well as inertial mechanism whereas both are particle inertia dependent. The theoretical study by Shobokshy and Ismail **[15]**, Wood **[16]** explains the dependency of rough surface for deposition. The experimental technique to investigate the deposition of submicron droplets on low pressure turbine blades can be found in the works of Parker and Lee **[17]**, Parker and Reyley **[18]** are noteworthy. The detailed work of Gyarmathy **[19]** and comprehensive study by Crane **[1]** on droplet deposition with relevance to steam turbine serves a good back ground for research as well.

From this background the aim of the thesis is to investigate the deposition on high stagger and camber angled turbine blades according to droplet size on non-equilibrium homogenous steam flow in last stage turbine cascade utilizing Eulerian-Eulerian approach in CFX. The deposition is not affecting the simulated flow but the deposition is purely calculated based on the simulated flow. Various new variables in terms of different equations implemented in CFD Post shall be observed for the effect of deposition on pressure side and suction side of the blades.

2 Mathematical Model

In the current work an Eulerian- Eulerian method is followed by means of Ansys CFX 15 code. Two dimensional compressible equation is solved for modeling two phase fluid where steam being the continuous phase and liquid being the droplet with phase change.

2.1 Governing Equations

Considering an arbitrary volume *V* with a differential surface area *dA*, the set of governing equations for mass, momentum and energy for the mixture liquid and vapor can be written as **[20]**:

$$\frac{\partial W}{\partial Q}\frac{\partial}{\partial t}\int Q dV + \oint M dA = \int N dV \qquad (2.1)$$

In the above equation *W*, *Q* and *M* can be defined as:

$$\begin{pmatrix} \rho \\ \rho u \\ \rho v \\ \rho E \end{pmatrix} \qquad \begin{pmatrix} P \\ u \\ v \\ T \end{pmatrix} \qquad \begin{pmatrix} \rho \boldsymbol{v} \\ \rho \boldsymbol{v} u + P\hat{\imath} - \tau_{xi} \\ \rho \boldsymbol{v} u + P\hat{\jmath} - \tau_{yi} \\ \rho \boldsymbol{v} E + P\boldsymbol{v} - \tau_{ij}\boldsymbol{v}_j - q \end{pmatrix}$$

The term *N* in equation (2.1) is the source term for body force and other energy sources.

The working fluid is the mixture of vapor-liquid and the conservation equation of the mixture can be determined from the following correlation as:

$$\phi_m = \phi_l\beta + (1-\beta)\phi_v \quad (2.2)$$

The ϕ from the above equation denotes h, s, C_p, C_v, μ.

The condensed liquid phase mass fraction and number of droplets per unit volume can be calculated as:

$$\frac{\partial \rho\beta}{\partial t} + \nabla.(\rho\vec{v}\beta) = \Gamma \quad (2.3)$$

$$\frac{\partial \rho\eta}{\partial t} + \nabla.(\rho\vec{v}\eta) = \rho I \quad (2.4)$$

In the above equations Γ, I represents the mass generation per unit volume and nucleation rate respectively. It is hypothesized that the interaction between droplets and vapor surrounding them is negligible which is quite good consideration as the size of the droplets are very small in the order of 1 μm or less.

2.2Nucleation and droplet growth model

According to the classical law of thermodynamics, the change in the Gibb's free energy ΔG is the reversible work required to form a single droplet of radius r from a supersaturated vapor of constant pressure p and at temperatureT_g. And change in Gibb's free energy is given by **[21]**:

$$\Delta G = 4\pi r^2\sigma - \frac{4}{3}\pi r^3\rho_l R T_g \ln S \quad (2.5)$$

The S in the above equation is the super saturation ratio. $S = p/p_s(T_g)$ and $p_s(T_g)$ is the saturated vapor pressure at T_g.

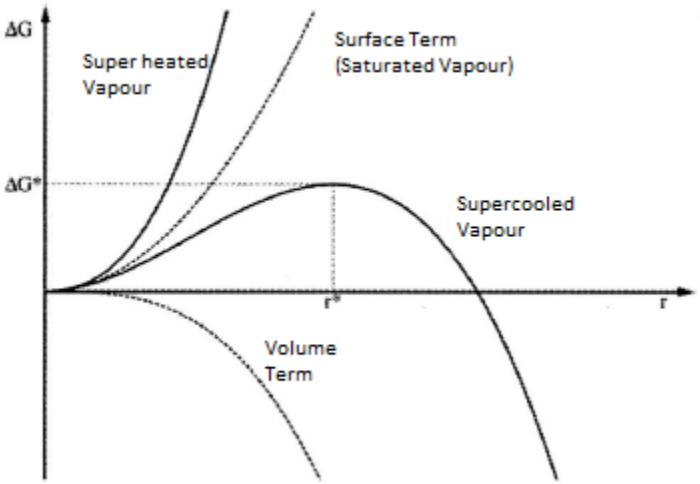

Figure 2: Variation of ΔG with r (modified) **[21]**

Figure 2 envisages the variation of ΔG with r. From figure 2 it can be seen that ΔG increases with increase in r up to a critical value of ΔG_* corresponding to critical radius of r_*. A droplet of radius $r > r_*$ has a tendency to reduce free energy of the system by capturing molecules and tends to grow.The opposite is true for $r < r_*$.

Considering the surface tension of the liquid be σ and liquid density $\rho_l$depend only on temperature and assuming that vapor behave as perfect gas the equation for ΔG_* and r_* can be derived from equation(2.5) as:

$$r_* = \frac{2\sigma}{\rho_l R T_g \ln S} \tag{2.6}$$

$$\Delta G_* = \frac{4\pi r_*^2 \sigma}{3} = \frac{16\pi\sigma^3}{3\left(\rho_l R T_g \ln S\right)^2} \tag{2.7}$$

A liquid droplet contains many H_2O molecules. Let a droplet of radius r contains g molecules can called as $g - mer$ and m be the mass of each molecule. Therefore, $\frac{4}{3}\pi r^3 \rho_l = gm$ and the surface area $4\pi r^2 = Ag^{\frac{2}{3}}$ where $A^3 = 36\pi\left(\frac{m}{\rho_l}\right)^2$. Substituting g in place of r in equation (2.5)

$$\frac{\Delta G}{kT_g} = \frac{A\sigma}{kT_g} g^{\frac{2}{3}} - g \ln S \tag{2.8}$$

$\ln S$ can also be written as:

$\ln S \cong \frac{h_{lg}}{RT_s(p)} \frac{\Delta T}{T_g}$ where h_{lg} is the specific enthalpy of evaporation.

In supersaturated vapor $S < 1$ growth of liquid droplets to macroscopic scale is prohibited even though small liquid like clusters are constantly formed and destroyed due to molecular collision process although size distribution remains steady. Size distribution of the cluster can be related as Boltzmann law as:

$$n_g \cong n_1 \exp\left(-\frac{\Delta G}{kT_g}\right) \tag{2.9}$$

The $n_g$and n_1 in the above equation represents numbers per unit volume of $g - mer$ and $mono - mar$. As the cluster concentrations remains steady in the system the balance equation or the kinetic equation can be written as:

$$C_g n_g = E_{g+1} n_{g+1} \tag{2.10}$$

And C_g represents the rate at which $g - mer$ acquires a molecule or alternately can be called as condensation rate whereas E_{g+1} is the rate at which $g + 1$ mar losses a molecule or evaporation rate. If the droplet exceed the critical size they encounter quite high ΔG gradient and has a tendency to grow and then no longer the kinetic equation is valid because the growth and decay of clusters are no longer balanced.

Let f_g be the concentration of $g-mer$ at the above given condition and I_g be the net rate per unit volume at which $g-mer$ grows to $g+1-mer$. Then I_g can be expressed as follows:

$$I_g = C_g f_g - E_{g+1} f_{g+1} \tag{2.11}$$

The time rate of change in the concentration of $g-mer$ can be written as:

$$\frac{\partial f_g}{\partial t} = -\left[\left(C_g f_g - E_{g+1} f_{g+1}\right) - \left(C_{g-1} f_{g-1} - E_g f_g\right)\right] \tag{2.12}$$
$$= -\left(I_g - I_{g-1}\right) \cong -\frac{\partial I_g}{\partial g}$$

C_g from the above equation can be expressed as:

$$C_g = q_c A g^{\frac{2}{3}} \frac{\rho_g \bar{v}_g}{4m} = q_c A g^{\frac{2}{3}} \frac{p}{\sqrt{2\pi m k T_g}} \tag{2.13}$$

Where q_c and $\bar{v}_g$ are condensation coefficient that is fraction of molecules incident to that of the absorbed on the surface and mean speed of vapor molecule respectively.

And E_g can be written as:

$$E_g = q_e A g^{\frac{2}{3}} \frac{p_s(T_l)}{\sqrt{2\pi m k T_g}} \exp\left(\frac{2\sigma}{\rho_l R T_l r}\right) \tag{2.14}$$

Here q_e is the evaporation coefficient.

For droplets in equilibrium $q_c = q_e$. For droplets in non-equilibrium$q_c \neq q_e$.

The change in $g-mer$ concentration can be approximated as:

$$\frac{\partial f_g}{\partial t} = -\frac{\partial I_g}{\partial g} = \frac{\partial}{\partial g}\left[c_g n_g \frac{\partial}{\partial g}\left(\frac{f_g}{n_g}\right)\right] \tag{2.15}$$

In steady state f_g varies only with g where all the large droplets are continually removed and replaced by equal mass of supersaturated vapor and therefore the system can remain in equilibrium without changing cluster distribution and nucleation rate.

If the case is considered to be isothermal then $T_l = T_g$. In general two phases are not in equilibrium so the temperature T_g and T_l are different from saturation temperature $T_s = T_s(P)$. $(T_s - T_g)$ which can also be called as vapor sub cooling is the measure of departure from thermal equilibrium. The droplet temperature can be given as **[24]**:

$$T_l = T_s - \frac{2\sigma T_s}{\rho_l h_{gl} r} \tag{2.16}$$

The above classical theory of nucleation and growth is simplified to two formulas that can be used wisely for the present work **[32]**

$$\Gamma = \frac{4}{3}\pi\rho_l I r_*^3 + 4\pi\rho_l \eta \bar{r}^2 \frac{\partial \bar{r}}{\partial t} \tag{2.17}$$

where

$$\frac{\partial \bar{r}}{\partial t} = \frac{P}{h_{lg}\rho_l\sqrt{2\pi RT}} \frac{\gamma+1}{2\gamma} C_p(T_l - T) \tag{2.18}$$

2.3 Properties of Fluid

The properties of fluid in case of two phase flow for water and steam is determined by IAPWS – IF97 in ANSYS CFX. This database has different formulations for five distinct thermodynamic regions of water and steam, namely:

Sub cooled water (1), Supercritical water/ steam (2), superheated steam (3), Saturation data (4), High temperature steam (5) as shown in figure 3.

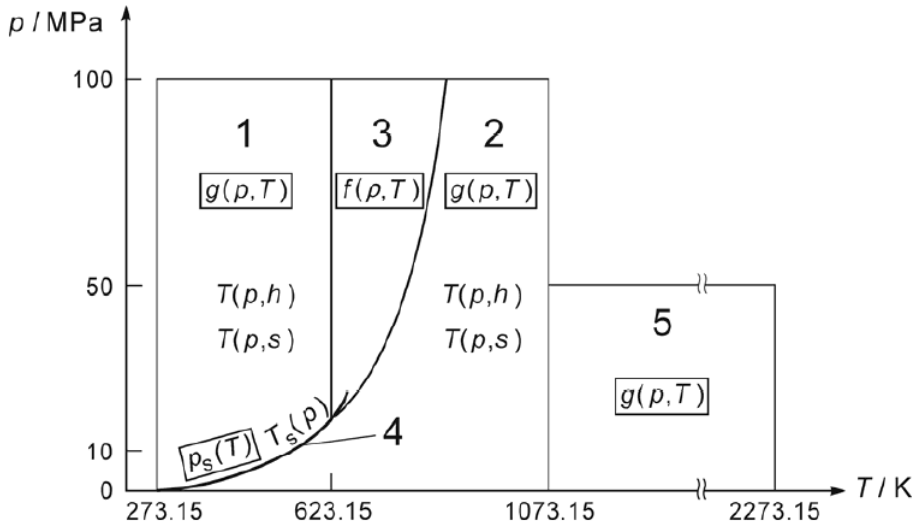

Figure 3: Thermodynamic Regions and Equations of IAPWS-IF97 **[31]**

The region 5 is not implemented in ANSYS CFX as it represents state at very high temperature and very low pressure. For this region CFX has other database. Region 1 and 2 are covered by individual specific equation of Gibbs free energy, region 3 by specific Helmholtz free energy. The reference state for IAPWS is triple point of water where internal energy, entropy and enthalpy are all set to zero.

The properties of the metastable state is obtained with the IAPWS extension where the equation of state is available for equilibrium phase change which can be used for the present case of droplet condensation. The equation of state for region 1 and 3 as shown in figure 3 of IAPWS-IF97 have reasonable accuracy for metastable state close to the saturation line. For the vapor condition under 10 Mpa in the region 2,

additional set of equations are used which matches well with saturation data. Above 10 Mpa, the equation of state for superheated region is extrapolated into super cooled region **[31]**.

3. Deposition Phenomenon

Sub-micron sized droplets are formed by rapidly expanding steam in steam turbine cascade. The deposition is quite significant in the ultimate stage of the steam turbine but the penultimate stage works normally in wet steam. The droplets are deposited on the blade surface resulting in film and are dragged to the trailing edge. These are broken in coarse droplets due to strong aerodynamic forces which fails to accelerate the vapor speed before impacting on the leading edge which is represented by the velocity diagram in figure 4.

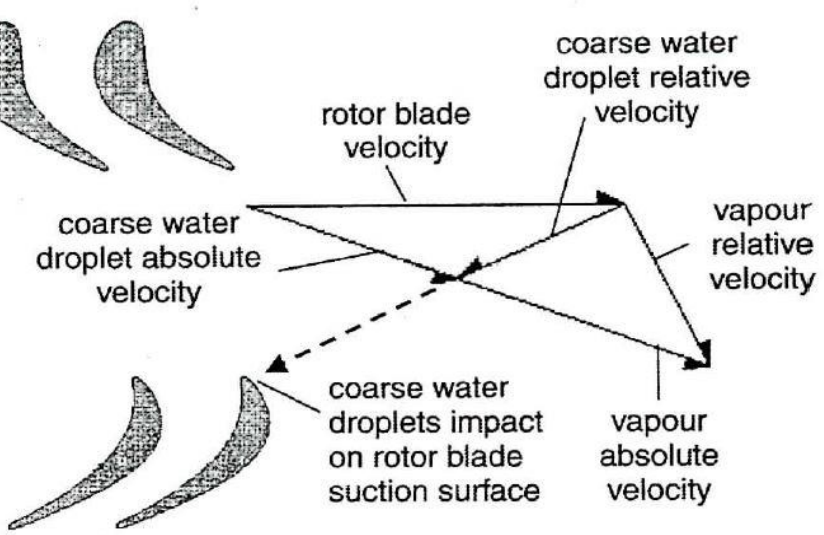

Figure 4: Velocity Diagram **[1]**

The deposition phenomenon can be described mainly by two mechanisms namely:

Turbulent Diffusion Mechanism

Inertial Deposition Impaction

3.1 Law of wall

Turbulent Diffusion Mechanism is a process by which the droplets entrained in the turbulent boundary layer migrates to the blade surface under the influence of the fluctuation of the flow.

To understand turbulent diffusion into more detail the law of wall has important role to play.

The relation between different parameters such as friction velocity u_τ, wall shear stress $\tau_w$and dimensionless wall distance y^+ are as follows **[27]**:

$u_\tau = \sqrt{\frac{\tau_w}{\rho}}$, $u^+ = \frac{u}{u_\tau}$ and $y^+ = \frac{y\, u_\tau}{\nu}$

As seen from the figure 5, there are four distinct regions namely viscous sublayer, buffer layer, log-law region and defect layer or outer layer **[27]**. Some brief description about the above mentioned layers shall be made in the following paragraph.

Viscous Sublayer: This is the inner most layer in the boundary layer such that $y^+ < 5$. This region is defined by the following equation: $u^+ = y^+$.

Buffer Layer: This region can be defined as $5 < y^+ < 30$. Neither of the following law holds good in this region $u^+ \neq y^+$ and $u^+ \neq \frac{1}{\kappa} ln\, y^+ + C^+$

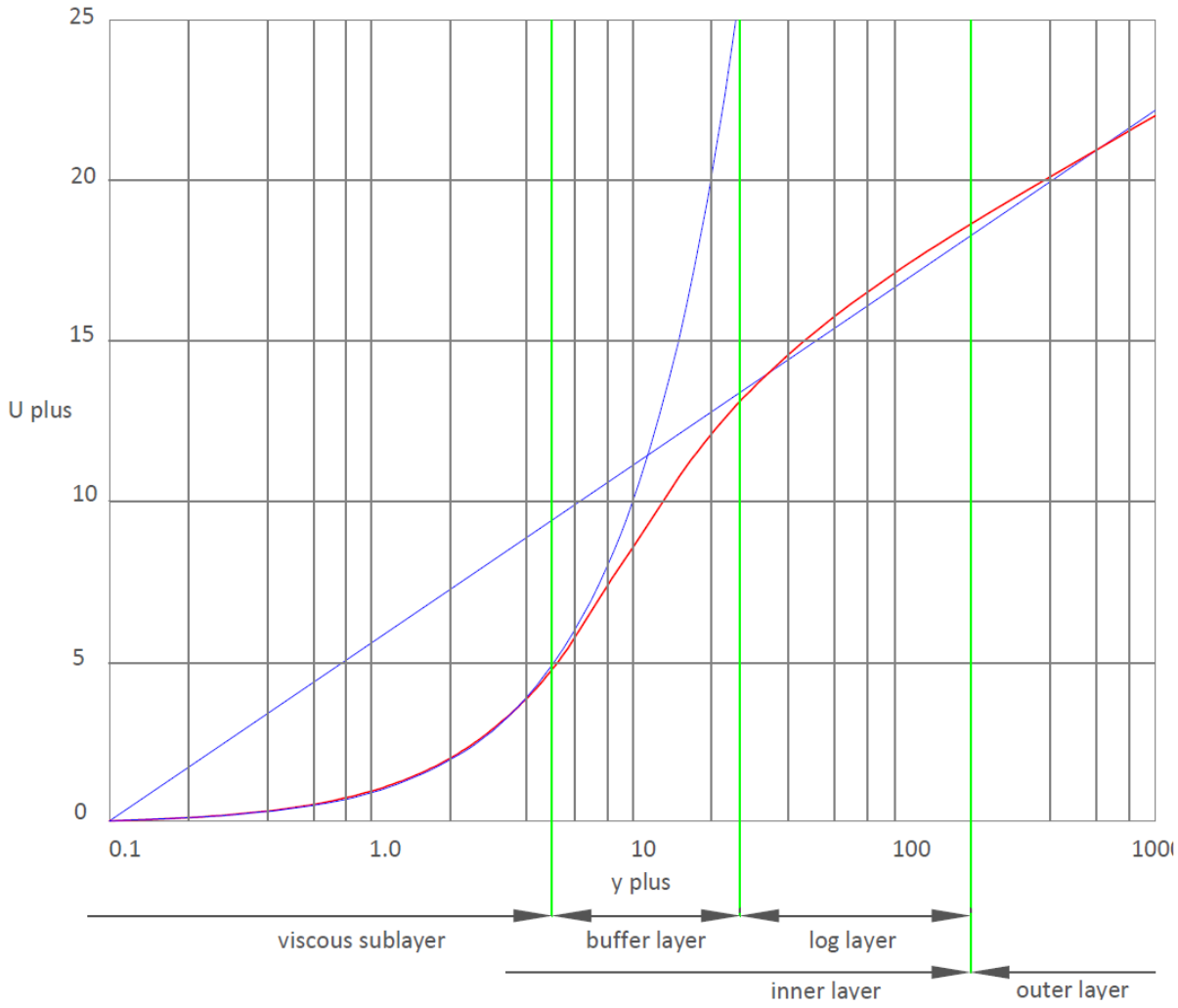

Figure 5: Law of Wall

Log-law Region: This layer starts after BL and extends up to defect layer. The following equation define the region: $u^+ = \frac{1}{\kappa} ln\, y^+ + C^+$

Defect Layer: This is region typically where $y^+ > 300$. Here, the effect of viscosity is negligible and the behavior of fluid is mostly controlled by free stream fluid.

3.2 Diffusional deposition mechanism

For the sake of simplicity the wet steam is considered to be the mixture of vapor and monodispersed droplets of radius r. When the steam passes through turbine blade some of the droplets will be deposited on the surface by turbulent diffusion through the boundary layer. Given that volumetric concentration of droplets outside the boundary layer to be $C_\infty$and mass transfer rate to the surface to be *N*. It is to be noted that both the above mentioned parameters vary with position on the blade surface.

When talking about mass transfer of droplets deposition velocity is an important parameter defined by *V* **[25]**, where

$V = {}^{N}/_{C_\infty}$

And dimensionless deposition velocity defined by V_+ can be written as:

$V_+ = {}^{V}/_{u_\tau}$

$V_+$is also the function of dimensionless inertial relaxation time of the droplets defined by τ_+.

$V_+ = f(\tau_+)$ (3.1)

Before defining τ_+, the definition of relaxation time must be mentioned. Actually, it is the time required by the droplets to accelerate to match the velocity of the vapor. Inertial relaxation time of the droplets defined by τ_r can be expressed as **[25]**:

$\tau_r = \frac{2\, r^2 \rho_l}{9\, \mu_g} (\phi(Re) + 2.7\ \mathrm{Kn})$ (3.2)

where $\mathrm{Kn} = {}^{l_g}/_{2r}$

$\tau_+ = {}^{\tau_r u_\tau^2}/_{\nu_g}$

$\phi(Re) = [1 + 0.197 Re^{0.63} + 0.00026 Re^{1.38}]^{-1}$

Equation (3.2) is a composite formula for spherical droplets where in the continuum regime (Kn<<1) it reduces to Stokes Law and in the free molecular regime (Kn>>1) it reduces to kinetic theory expression. Although the most of the calculation that have been developed for diffusional deposition is for turbulent pipe flow. However, these are well enough to understand the phenomenon in turbine blades. Three

deposition regimes can be identified namely: Turbulent Particle-Diffusion Regime, Eddy-Diffusion Impaction Regime, and Particle Inertia-Moderated Regime as in figure 6.

Turbulent Particle-Diffusion Regime: The regime is defined where $\tau_+ < 0.1$, here the particles are transported by Brownian and eddy-diffusion. The main resistance to mass transfer is in laminar sublayer where deposition rates are very low and decreases with increase in particle size. Here $V_+ = f(\tau_+, Sc)$ and Schmidt number is defined as: $Sc = {}^{\nu_g}/_{D}$

Eddy-Diffusion Impaction Regime: In this regime where $0.1 < \tau_+ < 10$, the deposition rate of the larger particle increases rapidly. The most probable theory behind this is that the particle are transported by intermittent turbulent bursts of fluid which disrupts the sublayer.

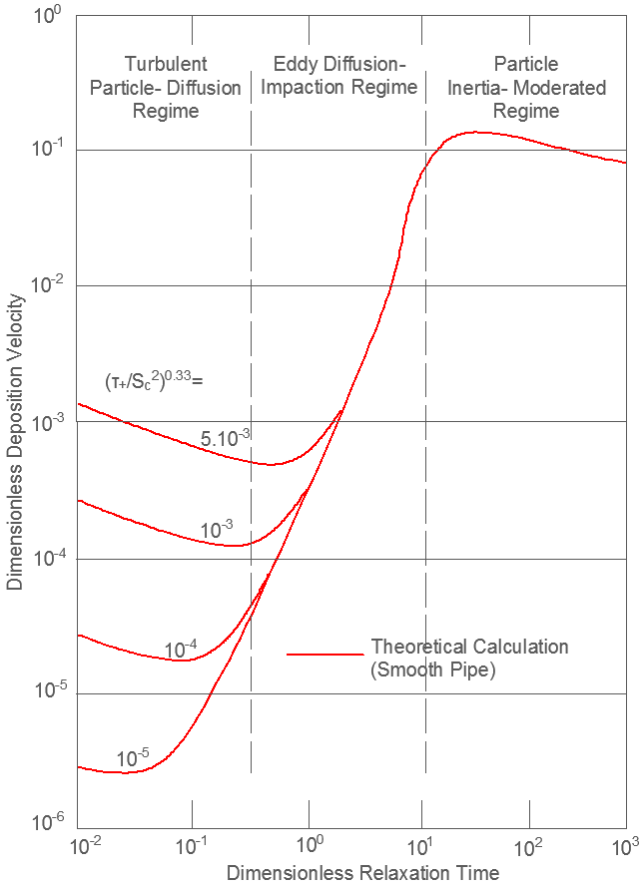

Figure 6: Diffusional Deposition Regimes in Turbulent Pipe Flow (modified) **[25]**

Particle Inertia-Moderated Regime: For very large particles where $\tau_+ > 10$, the deposition rate first increases then fall slightly. The transport rate through turbulent core of the boundary layer is reduced because the high inertia of the particle damps their response to the turbulent eddies.

The figure 7 describes the variation of inertial time with respect to droplet radius for different pressures. As droplet radius increases the inertial relaxation time also increases. As seen from figure 6, the inertial relaxation time is one of the most important parameter for the determination of depositional velocity and hence deposition.

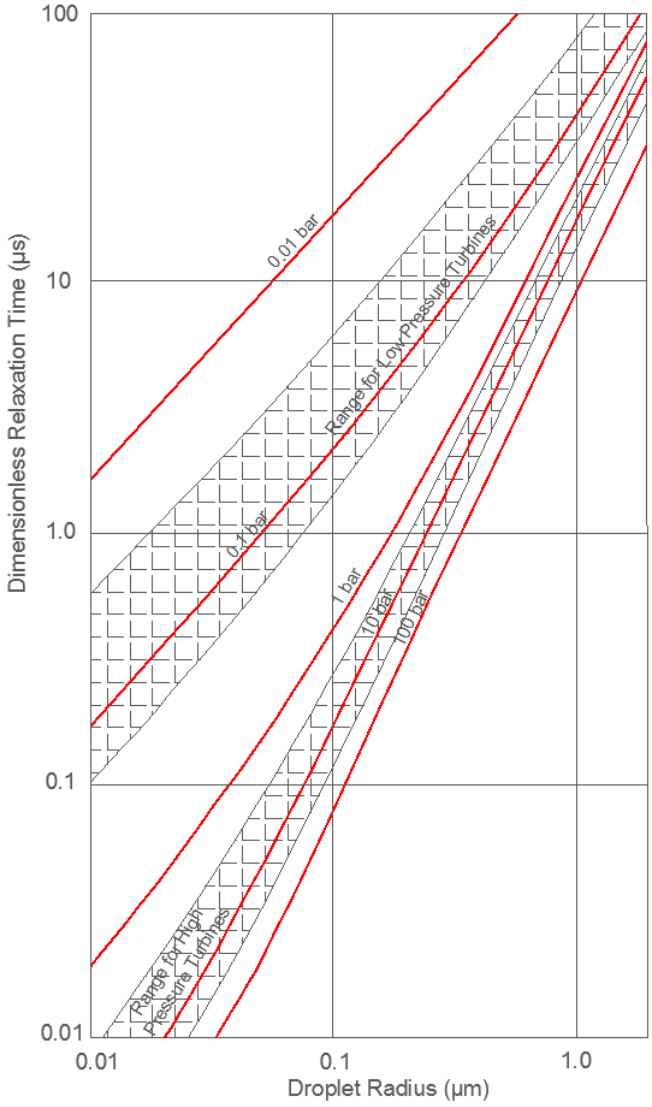

Figure 7: Inertial relaxation time of monodispersed water droplets in steam (modified) **[25]**

Actually the mass transfer rate of droplets on the surface can be calculated by integration of diffusion equation in the boundary layer. Mathematical model of deposition for three regions can be expressed under one equation as:

$$V_+ = \left(\frac{D}{\nu_g} + \frac{\epsilon}{\nu_g}\right)\frac{\partial c_+}{\partial y^+} \qquad (3.3)$$

where $c_+ = {C}/{C_\infty}$

Diffusional Coefficient of droplets *D* can be given by the equation:

$$D = \frac{K\,T_g}{6\,\pi r \mu_g}(1 + 2.7\text{Kn}) \quad (3.4)$$

In Turbulent Particle-Diffusion Regime and Eddy-Diffusion Impaction Regime the main resistance of diffusion is in Viscous Sub layer and Buffer Layer. Thus, for integration of equation (3.3) the limits of integration for outer layer are considered as $C_+ = 1$ and $y^+ = 30$. The integration limit for inner layer is difficult to define. In order to model the inertia coasting effect, the integration is stopped at a distance *s'* (stop distance) from the surface. According to Wood,

$$s^+ = \frac{s' u_\tau}{\nu_g} = 0.69\tau_+ \quad (3.5)$$

If the surface is rough,

$$b^+ = 0.45\frac{k_s u_\tau}{\nu_g} \quad (3.6)$$

Thus the limit of integration in the inner layer can be defined as:

$C_+ = 0,\ y^+ = s^+ + b^+ + r^+$ where $r^+ = \frac{k_s u_\tau}{\nu_g}$

In order to integrate equation (3.3) the relation between ${\epsilon}/{\nu_g}$ and y^+ must be known. Some measurements in turbulent flow pipes can be used for turbine blade as the main interest is near the wall where eddy diffusivity of the droplets is assumed to be equal to eddy viscosity of the fluid which means that Schmidt number to be unity.

Integration of equation (3.3) assuming V_+ to be constant can be written as:

$$V_+ = (I_S + I_B)^{-1} \quad (3.7)$$

where I_S and I_B represents the integral across the sublayer and buffer layer respectively. The equation of I_S and I_B is defined as follows:

For $(s^+ + b^+ + r^+) < 5$

$I_S = 14.5Sc^{2/3}[f(\phi) + g(\phi) - f(\phi_1) - g(\phi_1)]$

$I_B = 0$

For $(s^+ + b^+ + r^+) \geq 5$

$I_S = 0$

$I_B = 5\,ln\left[{25.2}/{(s^+ + b^+ + r^+ - 4.8)}\right]$

The $f(\phi),\ g(\phi),\ f(\phi_1),\ g(\phi_1)$ used for calculation of I_S for $(s^+ + b^+ + r^+) < 5$ are given below:

$$f(\phi) = \frac{1}{6}\left[\frac{(1+\phi)^2}{(1-\phi+\phi^2)}\right]$$

$$g(\phi) = \frac{1}{\sqrt{3}} tan^{-1}\left(\frac{2\phi-1}{\sqrt{3}}\right)$$

$$\phi = 5/a$$

$$\phi_1 = \frac{(s^+ + b^+ + r^+)}{a}$$

$$a = Sc^{-\frac{1}{3}}$$

The formulation in equation (3.7) can be used for $\tau_+ < 10$. For larger droplets in the inertia-moderated region i.e. $\tau_+ > 10$ the following equation can be used:

$$V_+ = 0.56\eta^*\, erfc\left(\frac{4.42}{\eta^*\tau_+}\right) \qquad (3.8)$$

where $\eta^* = \frac{\upsilon_l}{\upsilon_g}$

The relation between η^* and τ_+ can be shown in figure 8.

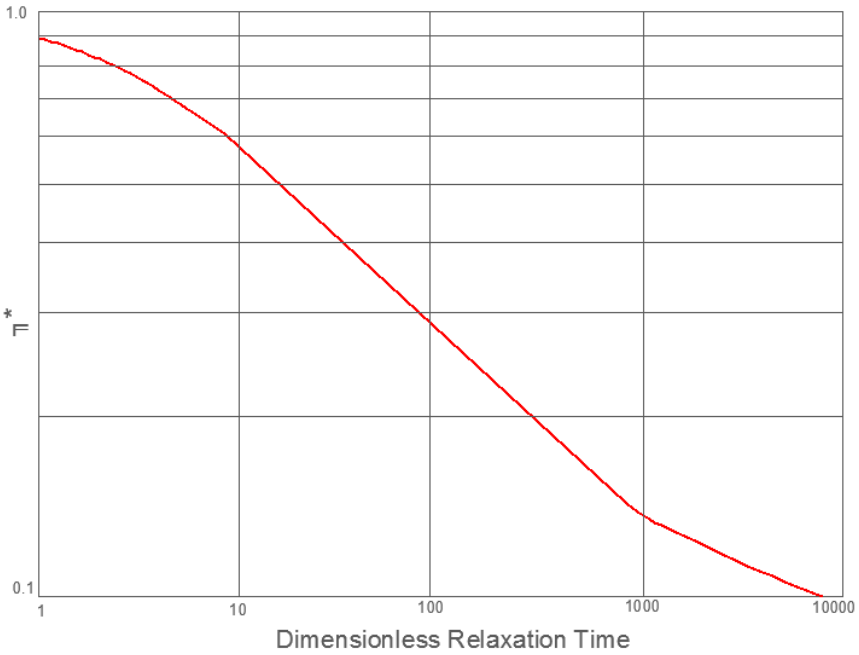

Figure 8: τ_+Vs ratio of droplet to gas RMS fluctuating velocity normal to the surface (modified) **[25]**

3.3 Inertial deposition mechanism

Fog droplets are assumed to be spherical particles moving in the flow field and are unaffected by particle-particle interaction, and the effects of condensation and evaporation is also neglected. Due to the

considerable difference in density between vapor and droplet only force that plays a crucial role is steady-state viscous drag force. Therefore, the equation of motion can be written as **[26]**:

$$\boldsymbol{D} = \frac{4}{3}\pi r^3 \rho_l \frac{d\boldsymbol{V}_l}{dt_l} \tag{3.9}$$

Here d/dt denotes the material derivative following a droplet i.e. $\frac{d}{dt} = \frac{\partial}{\partial t} + \boldsymbol{V}_l.\nabla$

The drag force $\boldsymbol{D}$depends on the flow regime and can be expressed as:

$$\boldsymbol{D} = \frac{6\pi\mu_g(\boldsymbol{V}_g - \boldsymbol{V}_l)}{[\phi(Re)+2.7\mathrm{Kn}]} \tag{3.10}$$

$$\phi(Re) = [1 + 0.197Re^{0.63} + 0.00026Re^{1.38}]^{-1}$$

Equation (3.10) is a composite formula for spherical droplets where in the continuum regime (Kn<<1) it reduces to Stokes Law and in the free molecular regime (Kn>>1) it reduces to kinetic theory expression.

$\frac{d\boldsymbol{V}_l}{dt_l}$ from equation (9) can be expressed as:

$$\frac{d\mathbf{V}_l}{dt_l} = \frac{\boldsymbol{V}_g - \boldsymbol{V}_l}{\tau_r} \tag{3.11}$$

$$\tau_r = \frac{2\,r^2\rho_l}{9\,\mu_g}(\phi(Re) + 2.7\ \mathrm{Kn})$$

Conceptually the trajectory of the particle introduced in the flow can be gathered by solving equation (3.11) for a given $\boldsymbol{V}_g$. But the problem arise due the mathematical stiffness to solve the above equation as inertial relaxation time τ_r is very small as compared to characteristic flow transit time, therefore integration increments Δt_l must be of the same order of τ_r.

One way to solve the above equation is to select Δt_l in such a way that it is large enough with respect to inertial relaxation time τ_r but small enough with respect to characteristic flow transit time where the averaged flow properties remains constant.

The right part of the equation 3.11 can be written in terms of slip velocity. Let the slip velocity be $\Delta\boldsymbol{V}$ and it can be written as:

$$\Delta\boldsymbol{V} = \boldsymbol{V}_g - \boldsymbol{V}_l \tag{3.12}$$

Combining equation (3.11) and (3.12) the following equation can be derived:

$$\frac{d}{dt_l}(\Delta\boldsymbol{V}) + \frac{\Delta\boldsymbol{V}}{\tau_r} = \frac{d\boldsymbol{V}_g}{dt_l} \tag{3.13}$$

The equation 3.13 can be integrated over a time step $\boldsymbol{\Delta t_l}$ provided $\frac{d\boldsymbol{V}_g}{dt_l}$ remains constant during the time step Δt_l.

$$\Delta\boldsymbol{V}_2 = \Delta\boldsymbol{V}_1 e^{-\left(\frac{\Delta t_l}{\tau_r}\right)} + \tau_r \frac{d\boldsymbol{V}_g}{dt_l}\left(1 - e^{-\left(\frac{\Delta t_l}{\tau_r}\right)}\right) \tag{3.14}$$

where 1 and 2 represent the start and end condition.

Changing the frame of reference

During calculation of droplet deposition on rotor blades it is convenient to work with frame of reference rotating same angular velocity **Ω** to that of the turbine. The vapor and droplet velocity with respect to the blade can be written as:

$$\boldsymbol{W}_g = \boldsymbol{V}_g - (\Omega X \boldsymbol{R})$$

$$\boldsymbol{W}_l = \boldsymbol{V}_l - (\Omega X \boldsymbol{R}) \quad (3.15)$$

where $\boldsymbol{R}$ is the position vector from origin of the coordinate system.

In rotating machines it is always easy to calculate in polar coordinate system(r, θ, z) as shown in figure 9. The three component of slip velocity in rotating frame of reference are given by:

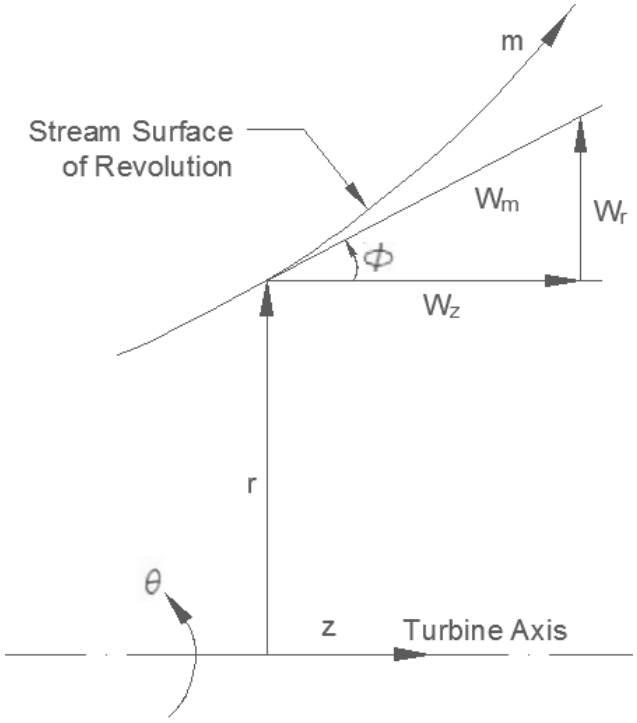

Figure 9: Meridional plane of frame of reference (modified) **[26]**

$$\Delta W_r = W_{gr} - W_{lr}$$
$$\Delta W_\theta = W_{g\theta} - W_{l\theta}$$
$$\Delta W_z = W_{gz} - W_{lz} \quad (3.16)$$

The three scalar equation of motion corresponding to equation (3.14) can be expressed by transform it into rotating coordinate system as:

$$\Delta W_{r2} = \Delta W_{r2}\beta + \tau_r(1-\beta)\left[\frac{dW_{gr}}{dt_l} - \frac{V_{l\theta}^2}{r}\right]$$

$$\Delta W_{\theta 2} = \Delta W_{\theta 2}\beta + \tau_r(1-\beta)\left[\frac{dW_{g\theta}}{dt_l} + \frac{W_{lr}W_{l\theta}}{r} + 2\Omega W_{lr}\right]$$

$$\Delta W_{z2} = \Delta W_{z2}\beta + \tau_r(1-\beta)\left[\frac{dW_{gz}}{dt_l}\right] \qquad (3.17)$$

$$\beta = \exp(-\Delta t_l/\tau_r)$$

The terms in the third bracket in equation 3.17 are the average terms which are constant over the increment Δt_l.

For making the calculation little bit simpler all the calculation are done in two dimensional assuming that the flow stream surface are surfaces of revolution with respect to turbine axis and fog droplet stream surfaces are identical to vapor stream surfaces.

Transforming the equation (3.17) into (m, θ) coordinate system results in:

$$\Delta W_{m2} = \Delta W_{m1}\beta + \tau_r(1-\beta)\left[\frac{dW_{gm}}{dt_l} - \frac{V_{l\theta}^2}{r}sin\phi\right]$$

$$\Delta W_{\theta 2} = \Delta W_{\theta 2}\beta + \tau_r(1-\beta)\left[\frac{dW_{g\theta}}{dt_l} + W_{lm}sin\phi\left(\frac{W_{l\theta}}{r} + 2\Omega\right)\right] \qquad (3.18)$$

where ϕ is the pitch angle of the stream surface in the meridional plane.

Figure 10 represents the computation grid with respect to equation 3.18 where m is the distance measured along stream surface in the meridional plane and θ is the circumferential coordinate as shown in the same figure.

$$\Delta W_m = \Delta W_{gm} - \Delta W_{lm} \qquad (3.19)$$

By setting $\Omega = 0$ the equations are applicable for stationary blade passages and by setting $\phi = 0$ the equations are suitable for two-dimensional calculations.

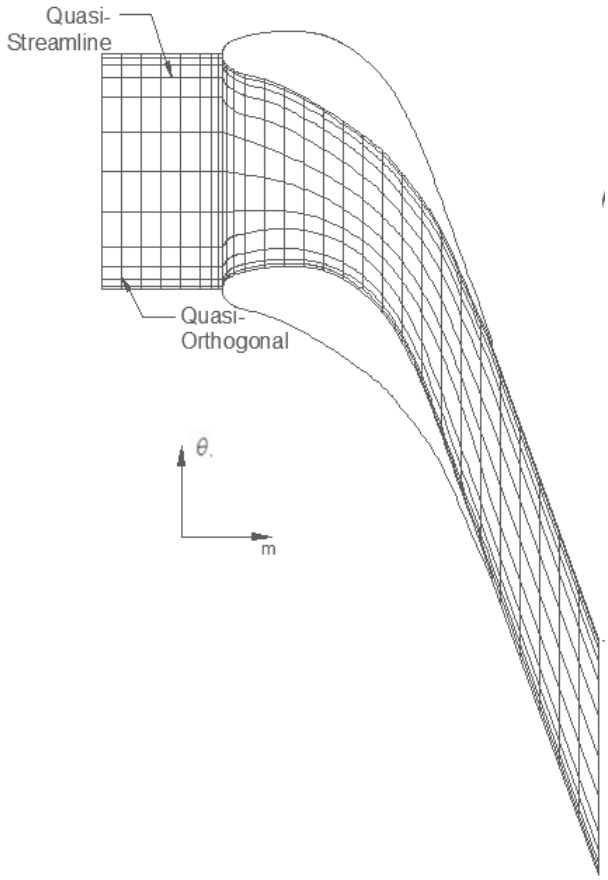

Figure 10: Representation of computational grid (modified) **[26]**

Simplified Theory of Deposition by Inertial Impaction

A Simplified Theory for Inertial Deposition proposed by Gyarmathy **[19]** based on inlet and outlet angle, chord length is quite efficient to calculate the deposition. The calculation is divided into two components where in the first the leading edge is considered to be a circular cylinder in a uniform parallel flow whereas in the second the pressure surface is considered to be parabolic profile in a flow with constant axial velocity. Although the Gyarmathy s theory comprises of two deficiencies firstly it does not include the rotational effect of rotor and secondly, the viscous drag on the droplet is considered to be independent of slip Reynolds number that causes a considerable error for large droplets. The mathematical formulation is divided into two sections where the first part discusses about the leading edge deposition and in the second part pressure surface deposition is discussed.

Leading Edge Deposition: The flow field is considered to be incompressible flowing uniformly over the circular cylinder. For Re<< 1, the collection efficiency η_c which can be defined as the ratio of deposited particle mass flux to incoming particle mass flux is the function of Stokes number as shown in the figure 11.

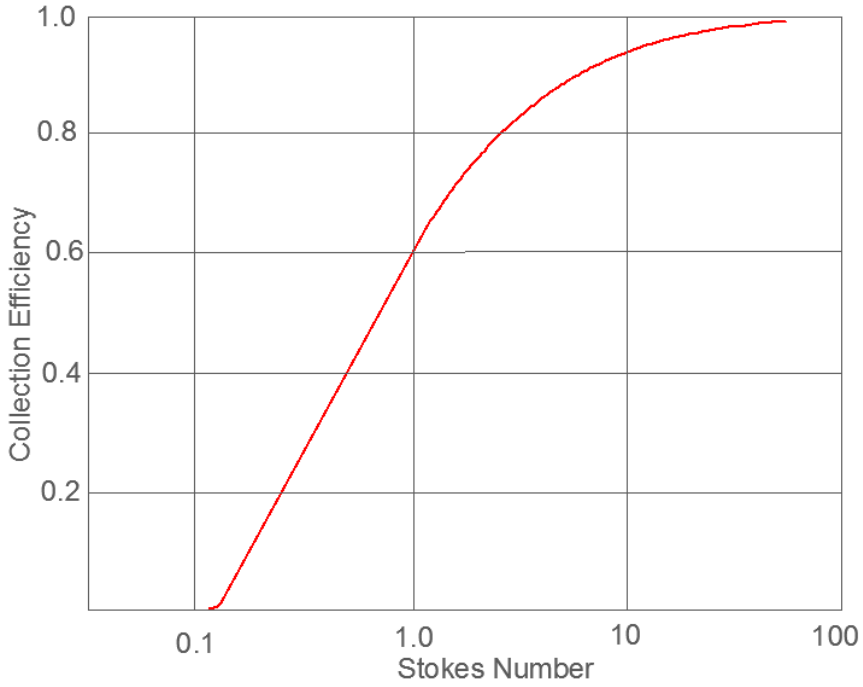

Figure 11: Collection efficiency Vs stokes number for a circular cylinder (modified) **[26]**

Thus, fractional deposition rate on the leading edge can be given as:

$$F_I = \eta_c \frac{2R}{P} \tag{3.20}$$

Where R is the equivalent leading edge radius and P is the pitch of the blade.

Pressure Surface Deposition: In this calculation the flow is considered to be two dimensional flow but inclined to a constant pitch angle ϕ with respect to the turbine axis.

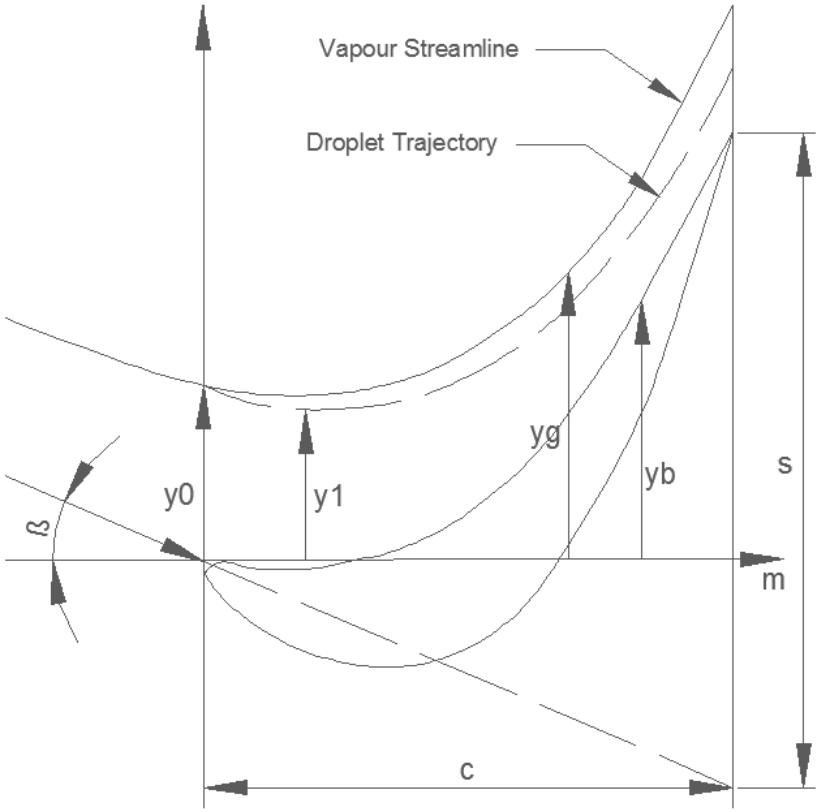

Figure 12: Geometric details of deposition on pressure surface (modified) **[26]**

The equation of stream line can be written by parabolic equation as:

$$y_g = y_0 - mtan\beta_0 + {sm^2}/{c^2} \tag{3.21}$$

Where c is the meridional chord, β_0 is the relative inlet flow angle and other notations as shown in figure 12.

Any variation in the meridional direction is not considered. The slip velocity in the circumferential direction can be written from equation (3.18) by neglecting $\frac{W_{l\theta}}{r}$ as:

$$W_{gy} - W_{ly} = \tau_r[\left(1 - \exp\left(-{m}/{W_m\tau_r}\right)\right].[W_m \frac{dW_{gy}}{dm} + 2\Omega W_m sin\phi] \tag{3.22}$$

The circumferential components can be written as:

$$W_{gy} = W_m \frac{dy_g}{dm}$$

$$W_{ly} = W_m \frac{dy_l}{dm} \tag{3.23}$$

by assuming $\Delta W_y = 0$ at $m = 0$.

Substituting equation (3.21) and (3.23) in equation (3.22), the equation for the trajectory of the droplet can be derived.

$$y_l = y_b + y_0 - 2s(St)(1-\alpha)\left[\left(\frac{m}{c}\right) - St\left(1 - e^{-m/cSt}\right)\right] \quad (3.24)$$

where y_b is the blade coordinate can be obtained by putting $y_0 = 0$ in equation (3.21). Stokes number St is given by $\tau_r W_m / c$ and the parameter α which represents the Coriolis acceleration on the droplet is given by $\frac{\Omega c^2 \sin\phi}{sW_m}$

The limiting trajectory that grazes the trailing edge on the pressure side of the blade can be obtained by setting $y_l = y_b$ at $m = c$. The y_0 is given as:

$$y_0 = 2s(St)(1-\alpha)\left[(St) - (St)^2\left(1 - e^{-1/St}\right)\right] \quad (3.25)$$

The fractional inertial deposition rate on pressure surface is given by:

$$F_I = \frac{2s}{P}(1-\alpha)\left[(St) - (St)^2\left(1 - e^{-1/St}\right)\right] \quad (3.26)$$

3.4 Thermophoresis deposition mechanism

Thermophoresis is the phenomenon which is observed due to temperature gradient in the free particles of different sizes and exhibit different response to the thermophoretic force. This phenomenon is observed in very small scale for example in the scale of one millimeter. Positive sign convention is applied when the particle move from hot to cold region and negative for reverse. Heavier particle exhibit positive thermophoretic force whereas lighter particle exhibit negative force. Although, the force is significant in smaller particle even with moderate temperature gradient. Figure 13 provides a concise idea about the deposition due to thermophoretic effect with respect to particle size and dimensionless relaxation time [**[22]**, **[23]**].

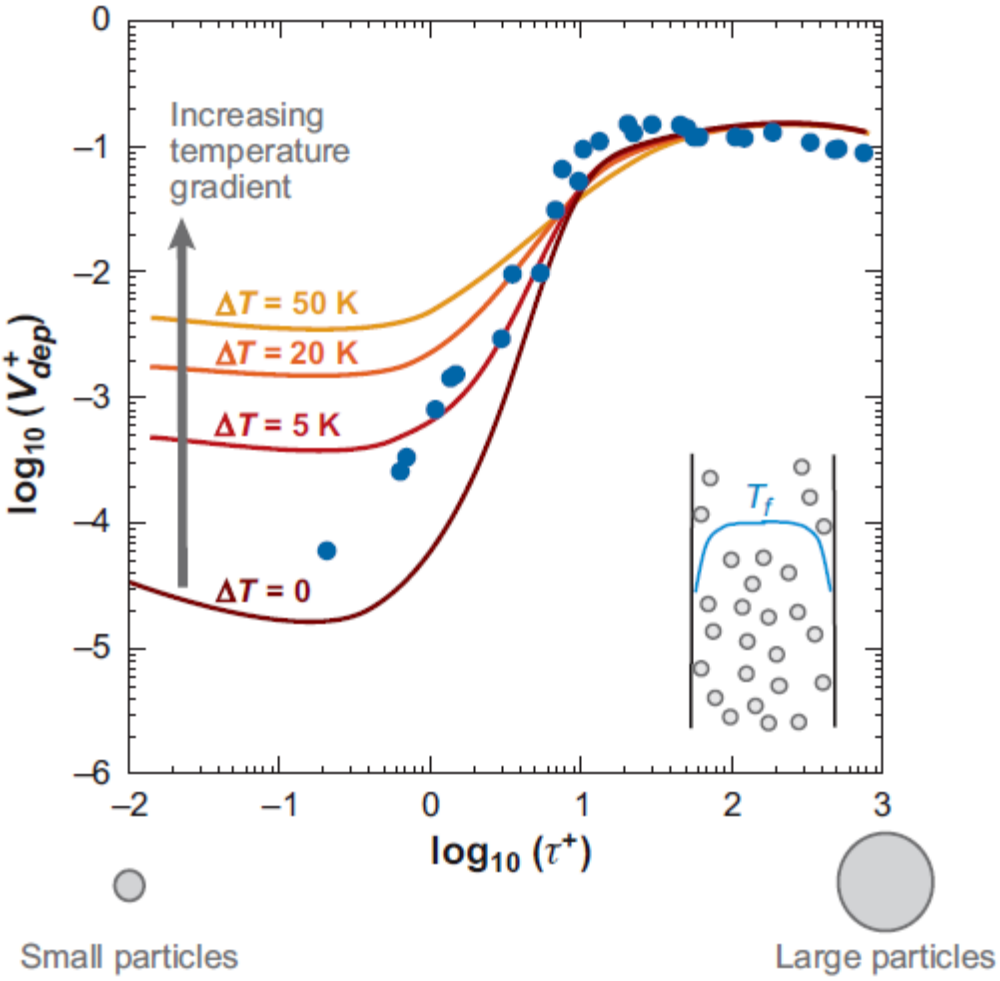

Figure 13: Thermophoresis effect on temperature gradient and particle size **[22]**

Few scientists such as Ryley and Davis took effort to encounter the problems due to deposition and they tested by internally heating the turbine blades. It is then when thermophoresis plays a dominant role. Although a great extent of work can be made to study deposition with combination of several phenomena along with thermophoresis but till now little is being studied on this part with respect to steam turbine. Currently, in the present work this phenomenon is not studied due to certain constrains but may be done in future works.

4. Deposition Experimental Observation

The remarkable experiment carried out by Crane **[1]** using a variable-incidence flat plate vertically in a wet steam tunnel. The sauter mean diameter was about 1 µm and the wetness fraction was calculated to be 2 percent in the steam tunnel. The deposition pattern was observed for an angle of zero incidence with

an elliptical nose as shown in figure 14. The designed plate can be imagined as a simple turbine blade. Although the modern day turbine blades profile is quite complex and three dimensional but the experiment work as presented by Crane **[1]** provides a good physical interpretation of deposition. Moreover, by changing the angle of incidence, the case is made familiar to the cascade condition at variable load when the flow condition is not similar to that of design condition.

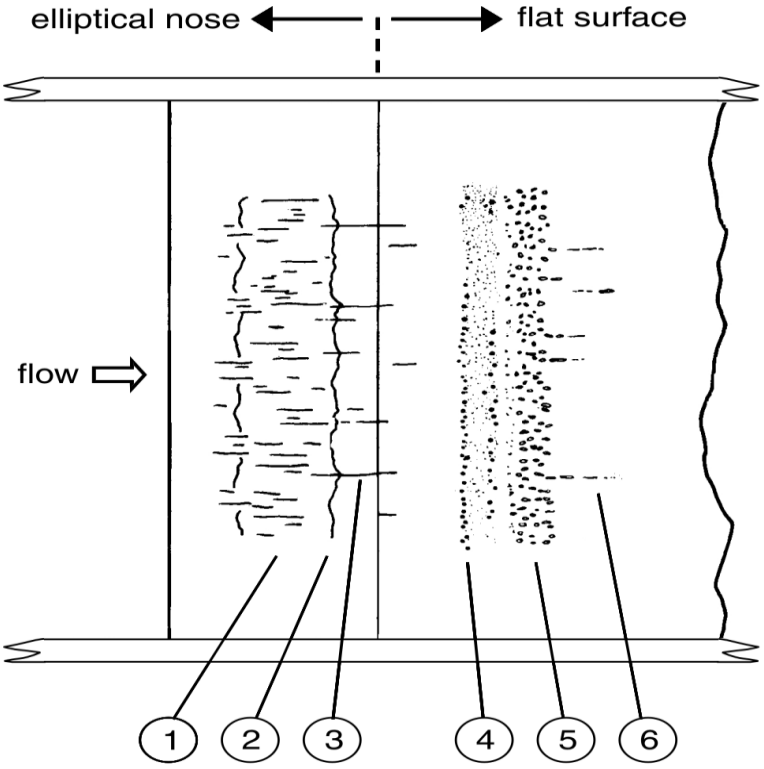

Figure 14: Fog droplets deposition pattern **[1]**

The observed pattern in deposition excellently described by Crane **[1]** are as follows :

"1. A thin surface film of water resulting from inertial deposition.

2. Apparent evaporation of the film, with occasional streaks.
3. Breaking away.
4. An unsteady zone of finely dispersed water, oscillating rapidly in the stream wise direction with an amplitude similar to its stream wise extent, about 5 mm.
5. A region of stationary globules, from the downstream end of which the globules either evaporated or were broken up and accelerated.
6. The pattern was similar with a sharp leading edge, except that feature 1 was absent."

5. Numerical Methodology

In the present study numerical calculation have been performed by steady state 2D Reynolds Averaged Navier Stokes equations in Ansys CFX. The mixture of liquid-vapor are discretized using conservative finite-volume integration over a control volume with a multi-grid method. Advection scheme and turbulence numerics are both set to High Resolution.

6. Results and Discussions

In this section detailed description of the results on deposition shall be made which are based on the mentioned theories. These are explained with the help of subsections such as the discussion of the test case, followed by grid independency test, and minute observation on deposition results.

6.1 Test Case Description

The turbine cascade data was taken from the paper of White et al. **[24]**, and the blade profile is a fifth stage stator blade of a six stage LP steam turbine of 660 MW. In the present study one specific case is chosen to investigate deposition on the blade surface. The detail about experimental condition of the selected case is provided in Table 1.

Table 1: Experimental Data

Upstream			Downstream
Stagnation Pressure P01 (mbar)	Stagnation Temperature T01 (K)	Stagnation Superheat T01-Ts (deg)	Mean Static Pressure P2 (mbar)
419	350	wet (1.6%)	178

The simulation is performed with five different droplet radius as inlet condition to observe the phenomenon of deposition depending on the droplet size. The different droplet sizes are illustrated in Table 2.

Table 2: Droplet Radius

Nomenclature	R1	R2	R3	R4	R5
Radius (μm)	0.4	0.6	0.8	1.0	1.2

6.2 Grid Independency

Grid independency test is very important to prove that grid has no effect on the solution. Apart from the grids presented here many more grids were created due to high complexity of the simulation. Table 3 describes three kinds of chosen grids namely Mesh 1, Mesh 2 and Mesh 3. From figure 15 shows pressure ratio in these three different grids. Mesh 1 solution is not at all satisfactory, whereas Mesh 2 and Mesh 3 are almost similar. Henceforth all the simulation shall be done with Mesh 2.

Table 3: Details of Final Grid

Mesh	Nodes	Elements	Aspect Ratio (Min.-Max.)	Skewness (Min.-Max.)	Orthogonal Quality (Min.-Max.)
1	39620	38875	1.81-8.33	2.69e-2-0.502	0.837-0.982
2	79140	78200	3.11-7.34	2.69e-2-0.503	0.7-0.983
3	93560	92600	4.54-10	2.68e-2-0.503	0.787-0.976

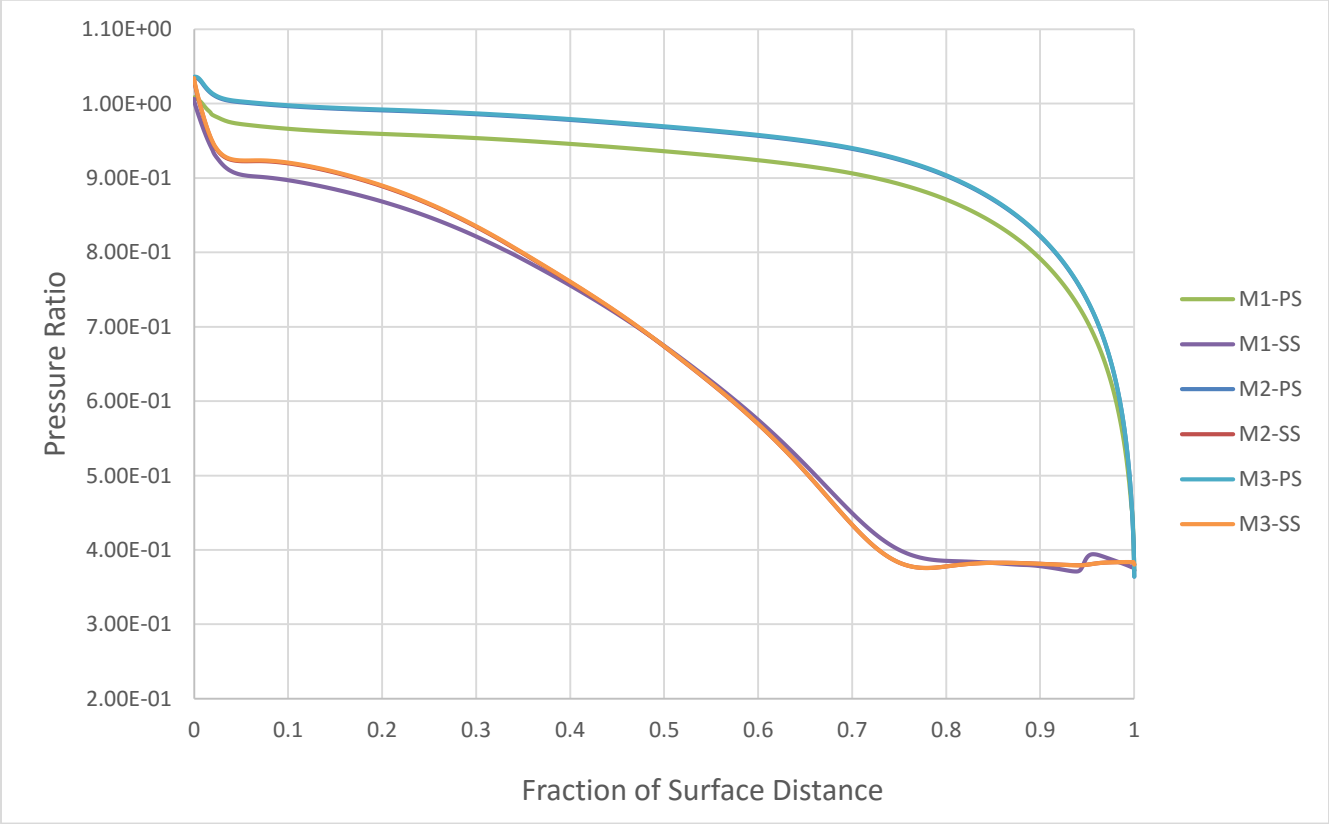

Figure 15: Grid Independency

The quadrilateral structured non uniform grid is generated with high refinement on the surface of the blade and few other regions in the flow domain as depicted in figure 16. The mesh is quite dense near the wall so that $y^+ \ll 1$ can be achieved as shown in figure 17. More details of the mesh quality are listed in Table 3.

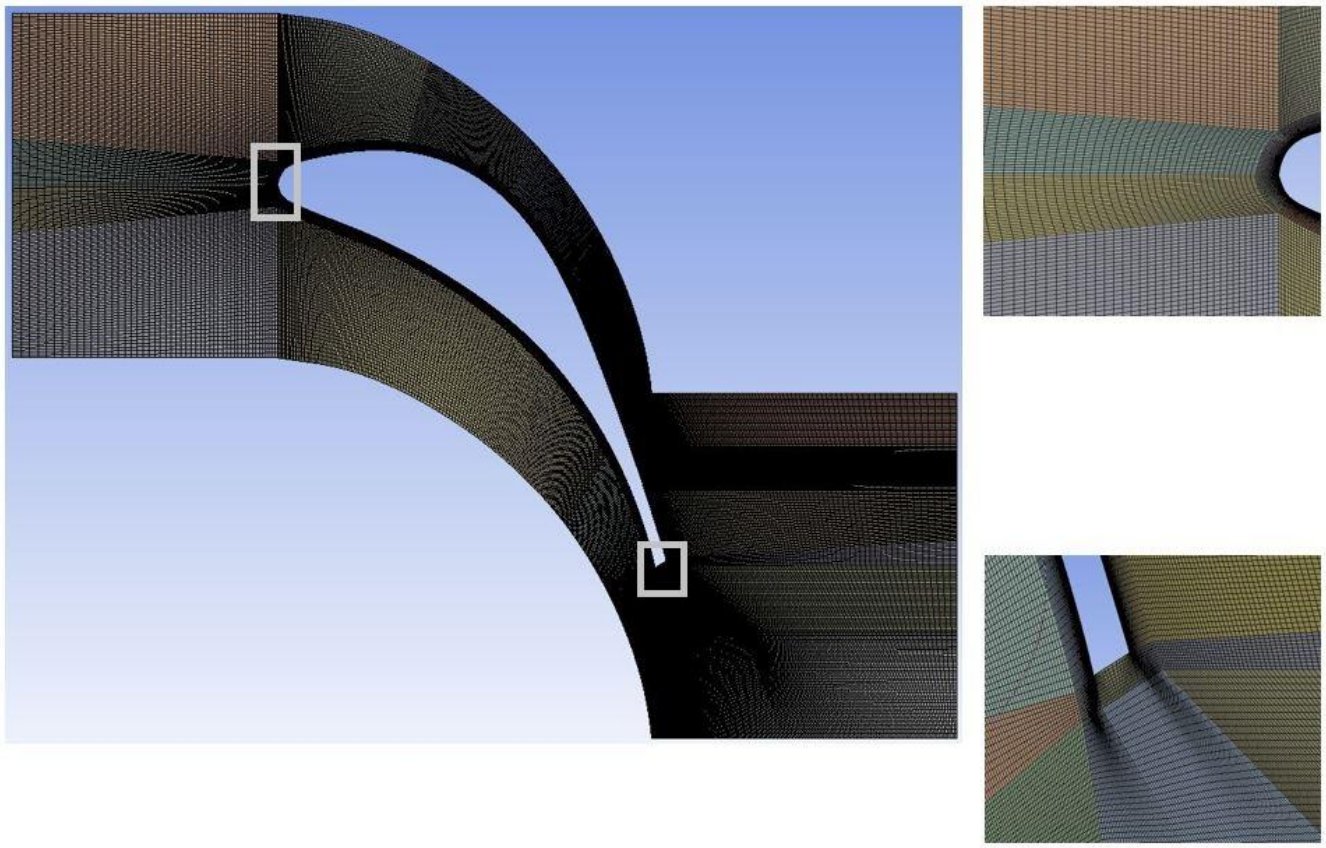

Figure 16: Computational Grid

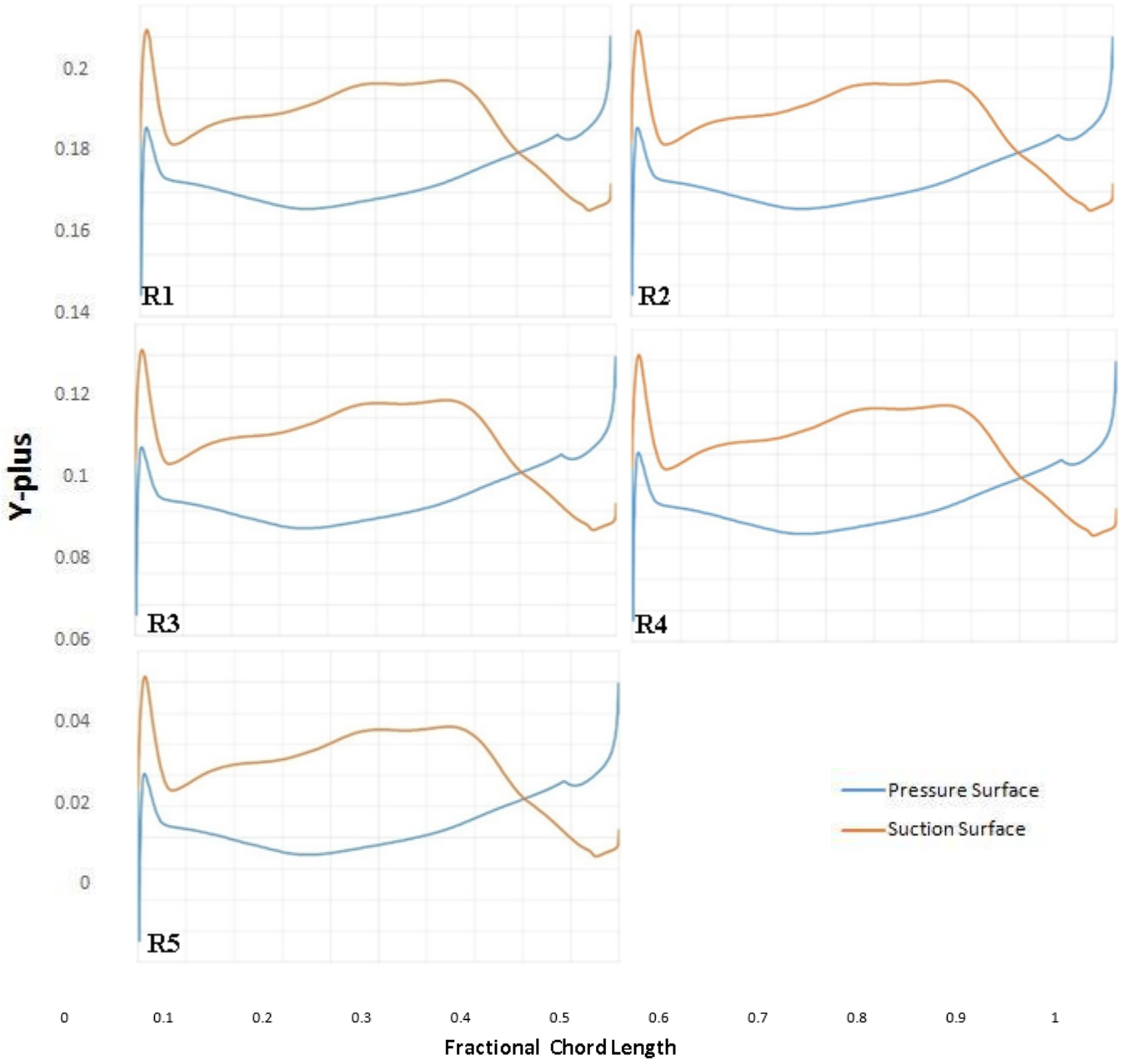

Figure 17: y-plus value

In the current work all the simulations have been done by $SST\ k-\omega$ model to simulate wet steam flow in the turbine cascade. The $SST\ k-\omega$ model is used for all the calculations. At first the simulation for equilibrium flows have been done. Then the result of the equilibrium flow is used as an initial condition for non-equilibrium flows of different droplet sizes as the inlet condition whereas pressure and temperature of inlet and outlet remains the same as in equilibrium simulation. In equilibrium calculation it is assumed that the two phases are in same temperature, whereas in non-equilibrium the above

condition do not hold good. Simulation for non-equilibrium condition with equilibrium result as initialization provides a good initial condition for further simulation and makes the process simple as well serves good both in terms of accuracy and computational time.

Convergence- It is assured that the solution presented in the current work were converged to normalized RMS residuals of the order of 10^{-5} or lower. This convergence criterion is maintained for all the simulations. Figure 18 shows the convergence for mass and momentum, imbalance respectively. The discontinuity in all convergence plots are due to the usage of equilibrium result as the initial condition for the simulation of non-equilibrium calculations. Almost all the variables in the iteration have converged to the order of 10^{-5} or below.

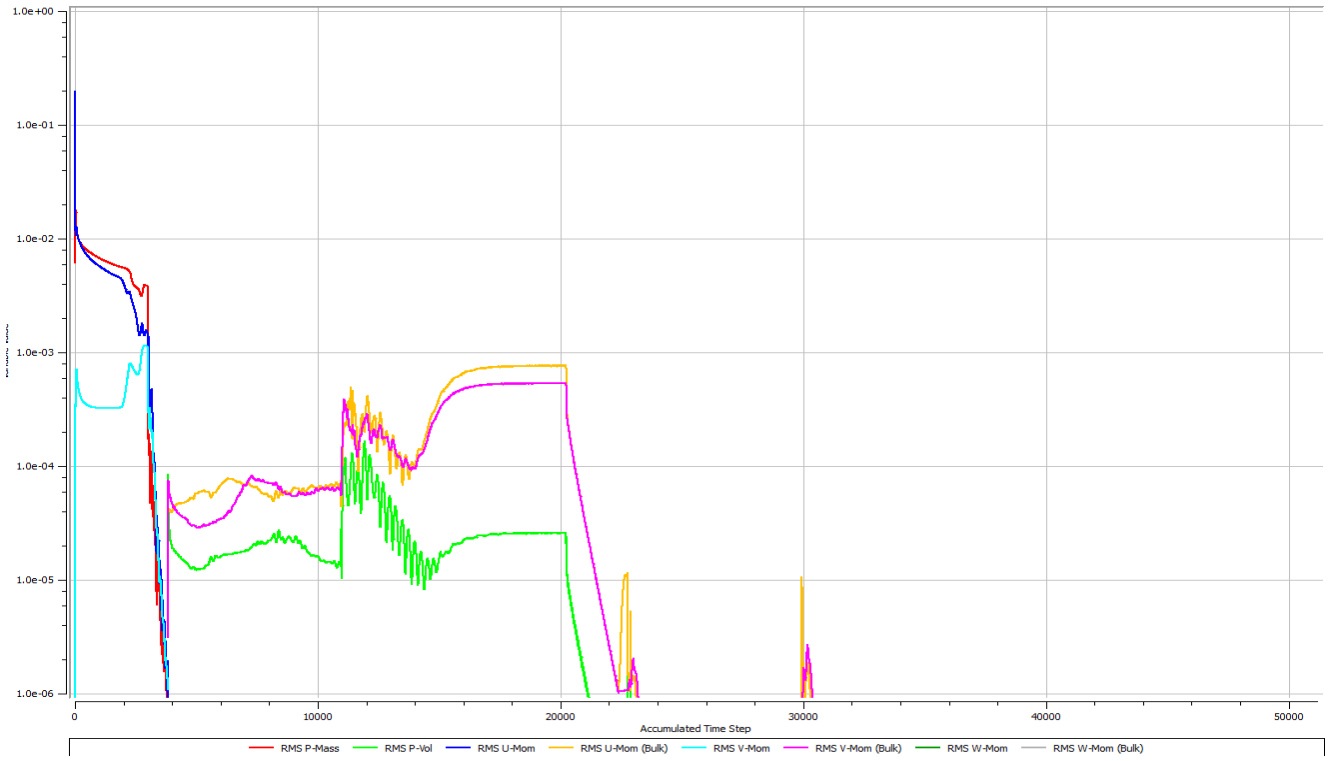

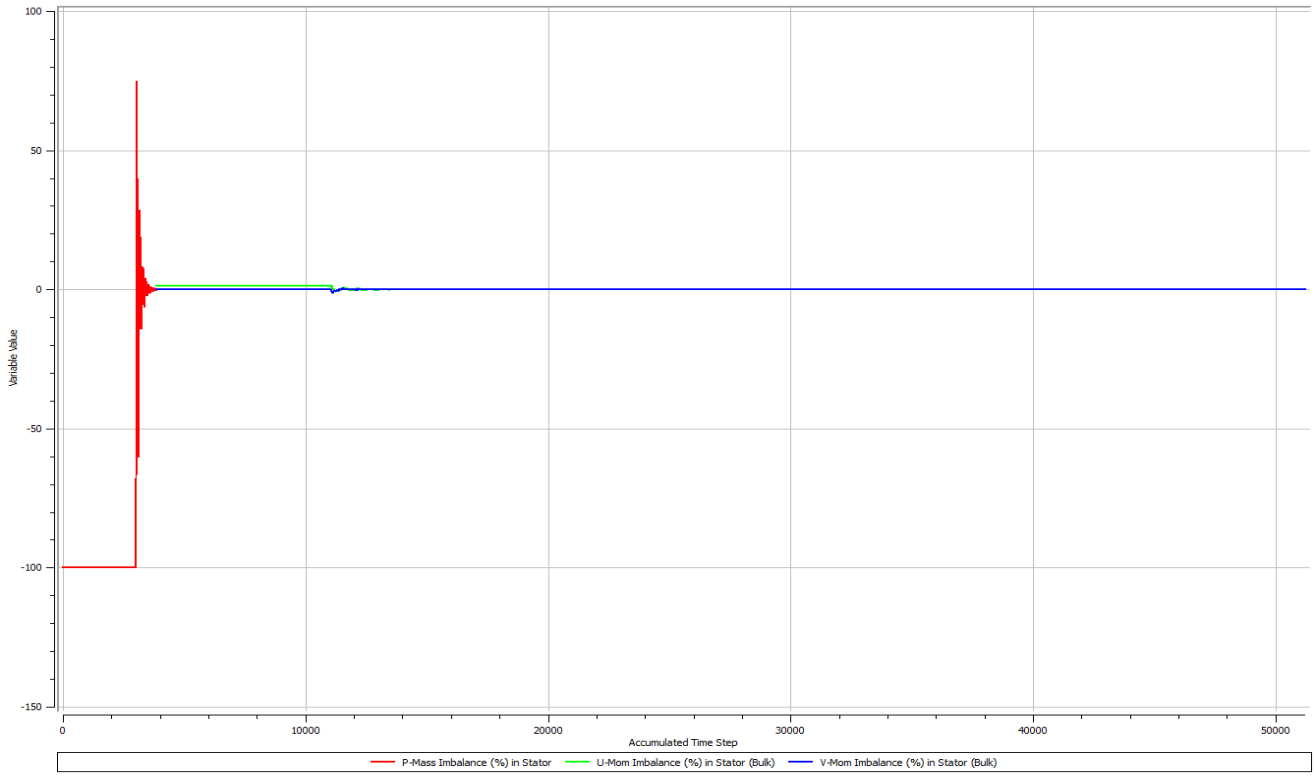

Figure 18: Convergence Criteria

6.3 Flow Field Description

Figure 19 envisages the pressure distribution on the blade surface namely suction side and pressure side and the results are compared with experimental results by White et al. **[24]**. The study is carried on by five different mono dispersed droplets namely R1, R2, R3, R4, R5 respectively as described in table 2. In the experiment of the particular case it was observed that there is strong bimodal droplet size distribution, indicating that secondary nucleation occurred in the cascade. The mean radius of the larger droplet mode was found to be around 0.5 µm.

The pressure distribution according to calculation has certain amount of deviation from the experimental result. This is because condensation of primary droplets was enough to arrest excessive departures from equilibrium and therefore the secondary nucleation was less intense and continued for a longer period. Moreover, the calculation does not consider slip between vapor and droplets although there is considerable slip for larger droplets with vapor phase.

The pressure distribution throughout the domain for all simulations with different radius in figure 20 appears to be almost similar. Therefore, it is observed that different droplet radius has almost negligible influence on the pressure distribution. The steam is expanding through the stator at expense of pressure drop. The pressure side pressure distribution is high as compared to suction side pressure distribution.

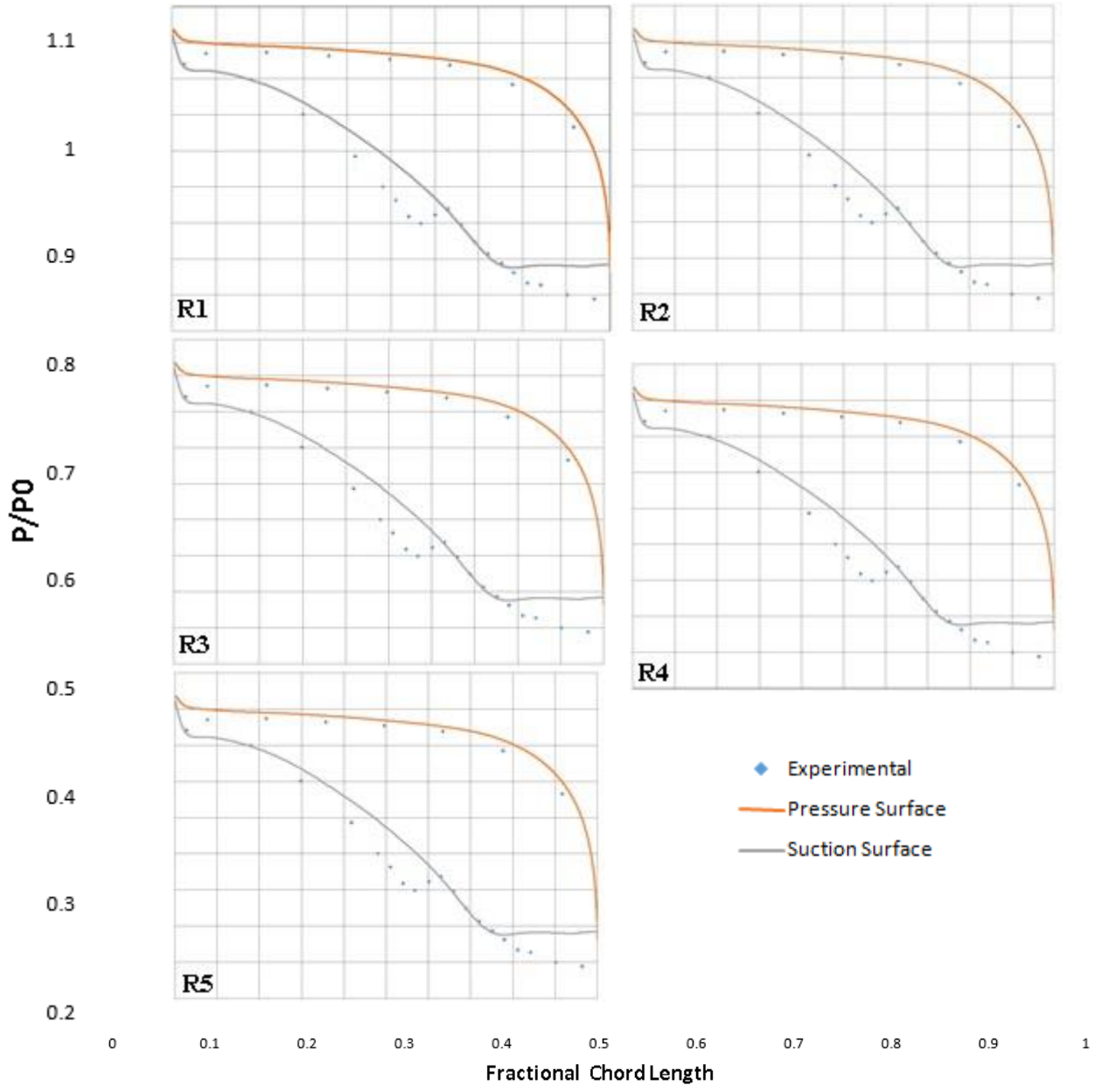

Figure 19: Blade Surface Pressure Distribution

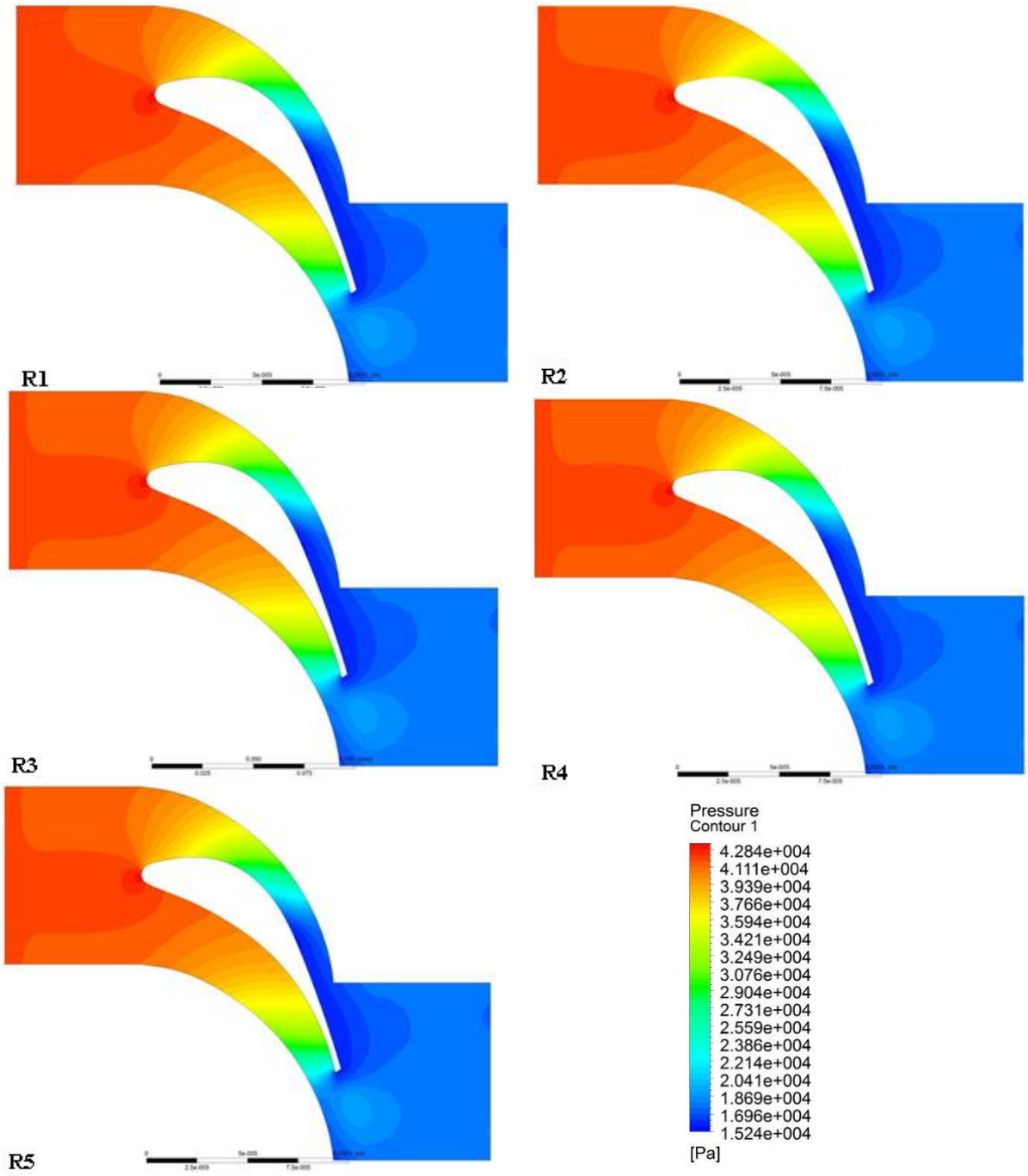

Figure 20: Pressure Contour

Figure 21 shows the temperature plot for each of the condition. The steam is expanded through the stator blades and energy is getting decreased, therefore temperature is gradually decreased through the blade passage. The size of the droplet has no appreciable effect on the temperature distribution. It is found that average outlet temperature to be same about 377.7 K for all the conditions.

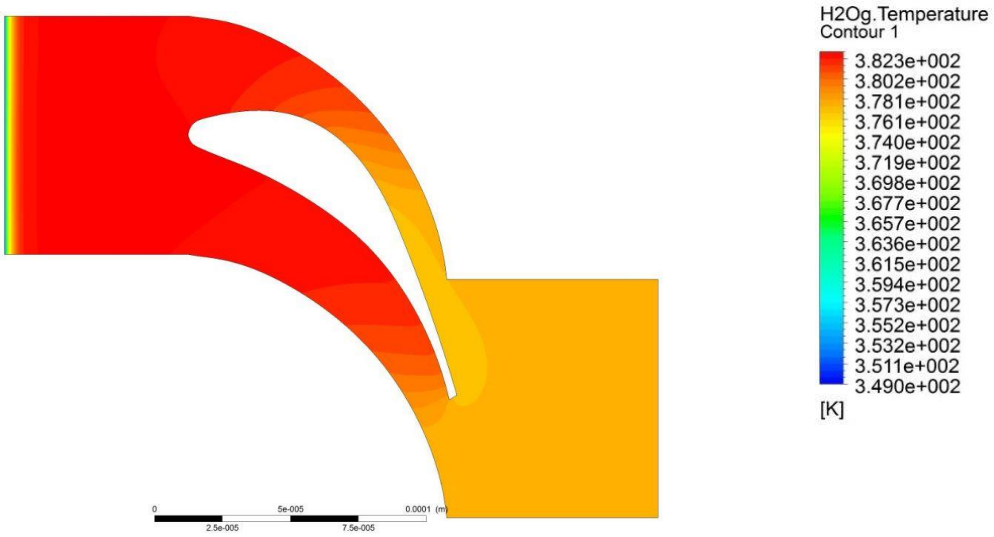

Figure21: Gas Temperature Contours

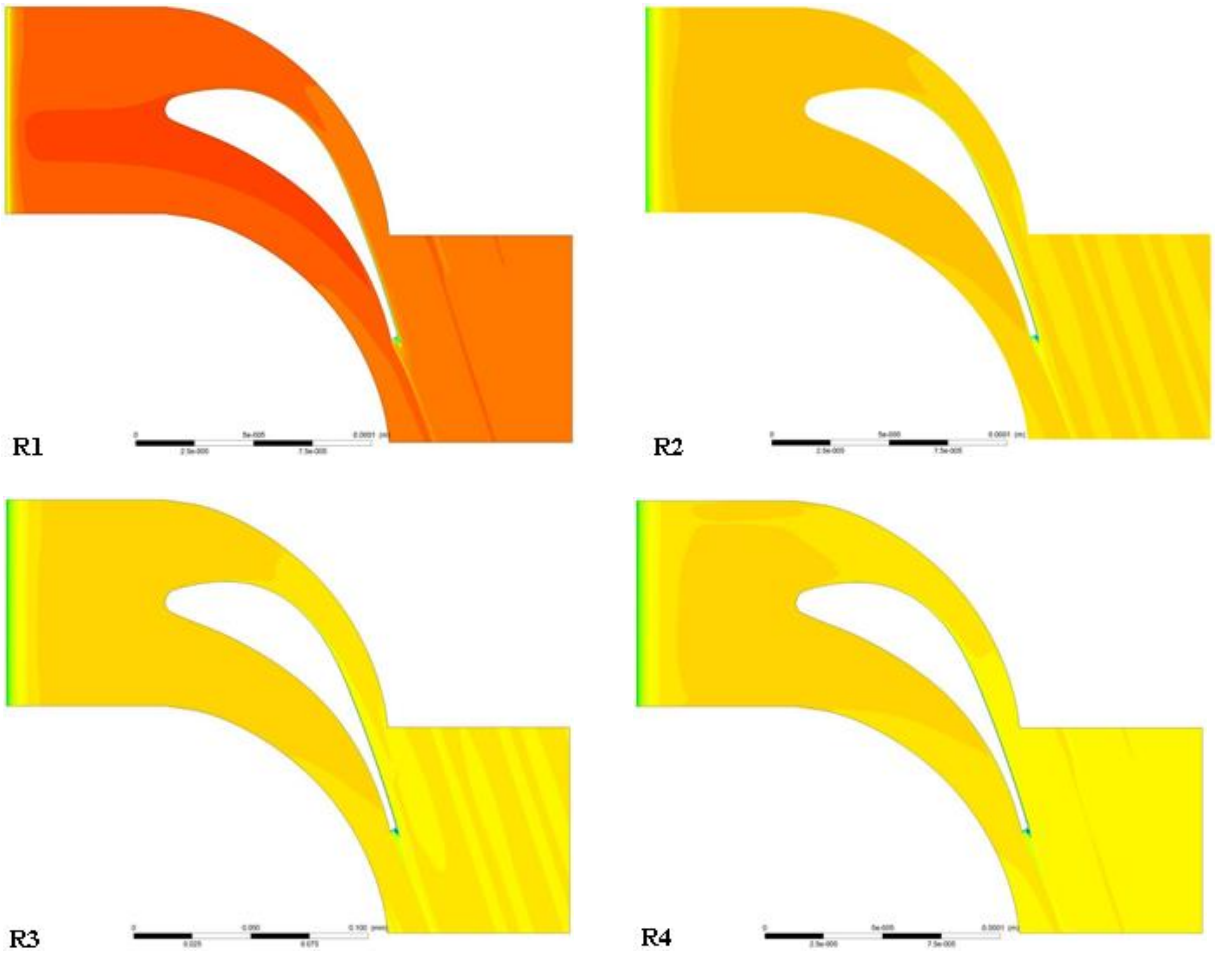

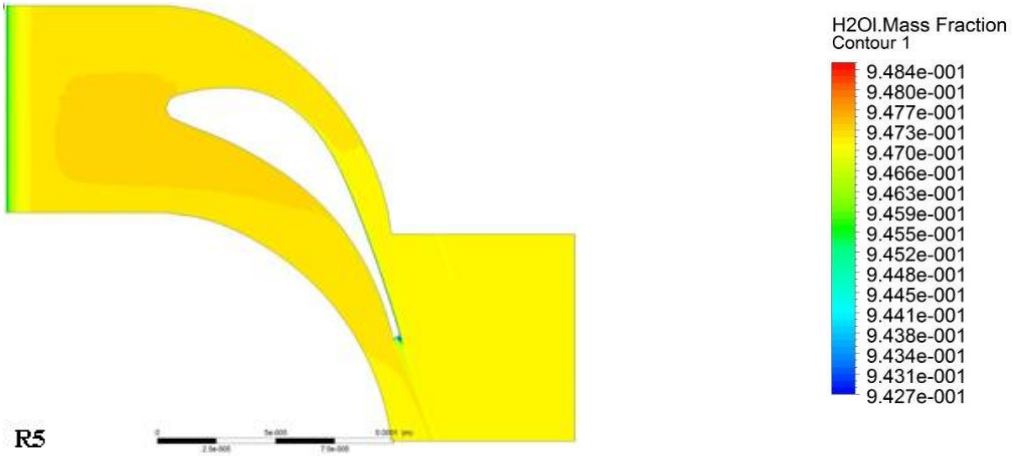

Figure 22: H_2Ol Mass Fraction Contours

Figure 22 depicts the contours for H_2Ol mass fraction and here the noticeable difference can found according to droplet radius. The physics behind this can be explained by the help of a mathematical formula.

$$\eta = \frac{\beta}{(1-\beta)V_d\left(\rho_l/\rho_g\right)}$$

where η is the number of droplets per unit volume,

$V_d = \frac{4}{3}\pi\bar{r}_d{}^3$ and β is the wetness fraction.

Therefore wetness fraction remaining constant, $\eta \propto 1/\bar{r}_d{}^3$

Mass fraction distribution for smallest radius in figure 22 is highest and gradually decreases with increase in droplet radius.

The same reason holds good for droplet number plot in figure 23. The droplet number for R1 which is the smallest droplet size is highest and decreases with the increase in droplet size. The distribution of droplet number throughout the computational domain can be seen from the plots.

The flow across the turbine cascade is well established and matches suitably with previous studies although with some discrepancies. Here after the phenomenon on deposition shall be discussed in detail. Two prominent kind of deposition physics are turbulent diffusion type and inertial deposition type.

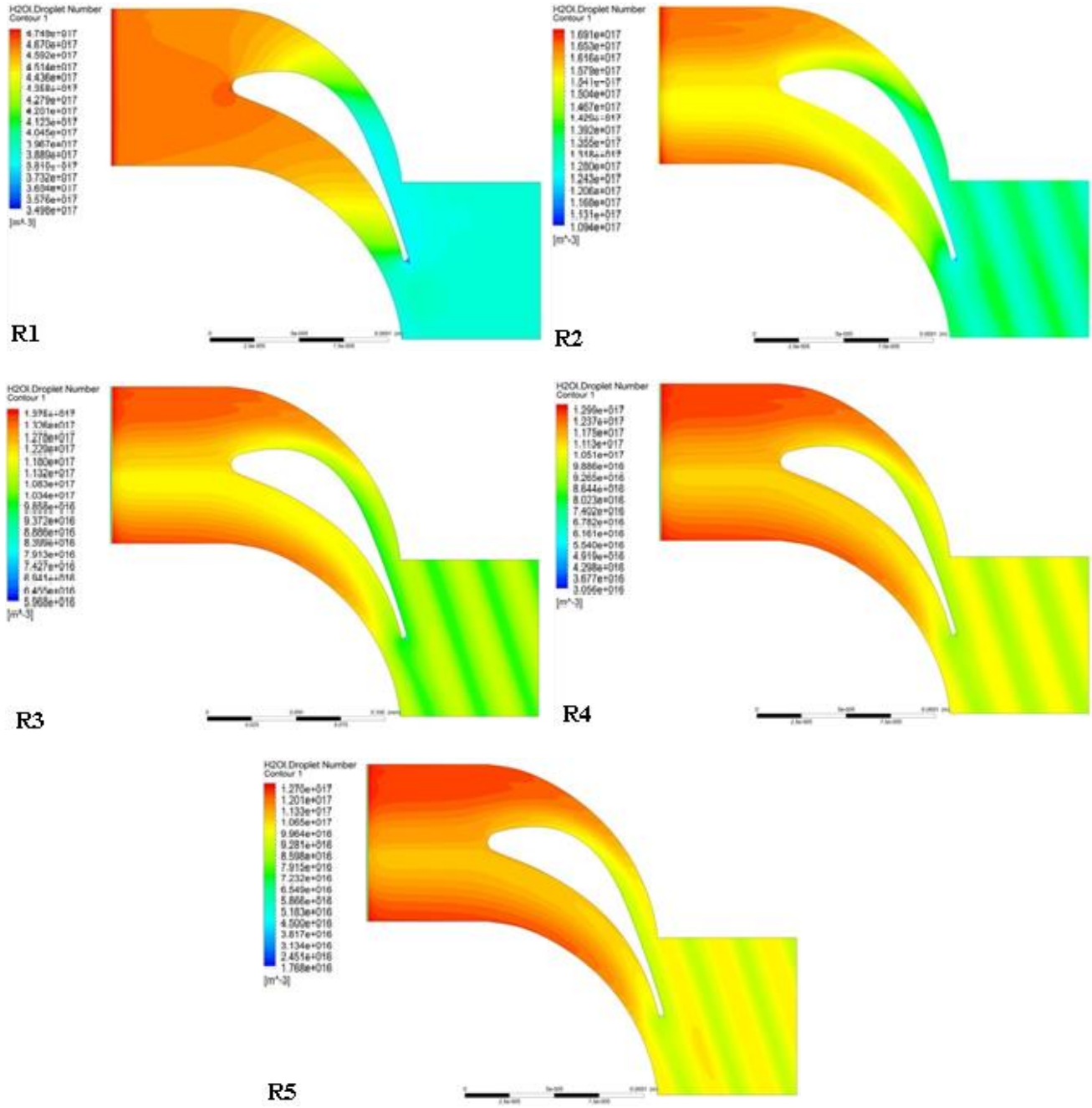

Figure 23: H_2Ol Droplet Number Contours

6.4 Turbulent Diffusion Deposition

The main challenge to compute diffusional deposition lies in the correct prediction of boundary layer. The flow within the cascade lies within eddy-diffusion impaction regime and with the small changes in u_+ there is a large change in V_+. Moreover, it is very difficult to find the boundary layer over the blade mainly because of the complex blade geometry and complex varying flow field within the cascade. The

calculation of deposition is only possible if the droplet concentration can be known at the outer edge of the boundary layer.

The prediction of boundary layer was completed in two attempts. In the first attempt the prediction is based on the fact of existing strong velocity gradient in the boundary layer whereas in the second the prediction is based on the concept of vorticity. Although the first method was not quite successful, but the second method for prediction of boundary layer was accurate and further calculations are performed with the second method.

In the first method, the boundary layer is calculated by introducing a new variable BL in CFD-post. The BL can be defined as follows.

$$BL = \left(\frac{\partial u}{\partial x} + \frac{\partial v}{\partial x} + \frac{\partial w}{\partial x}\right)\hat{\imath} + \left(\frac{\partial u}{\partial y} + \frac{\partial v}{\partial y} + \frac{\partial w}{\partial y}\right)\hat{\jmath} + \left(\frac{\partial u}{\partial z} + \frac{\partial v}{\partial z} + \frac{\partial w}{\partial z}\right)\hat{k}$$

The concept behind introduction of BL lies in the fact that within the boundary layer of the turbine blade there lies a strong velocity gradient as indicated in figure 24. Outside the boundary layer the BL remains almost constant. With little amount of post processing the boundary layer for each simulation is calculated as depicted in figure 25. The coordinates of the outer edge of the boundary layer was collected and implemented as polylines in CFD Post to compute the droplet number the outer edge of the boundary layer. The detail of post processing is shown in Appendix 1.

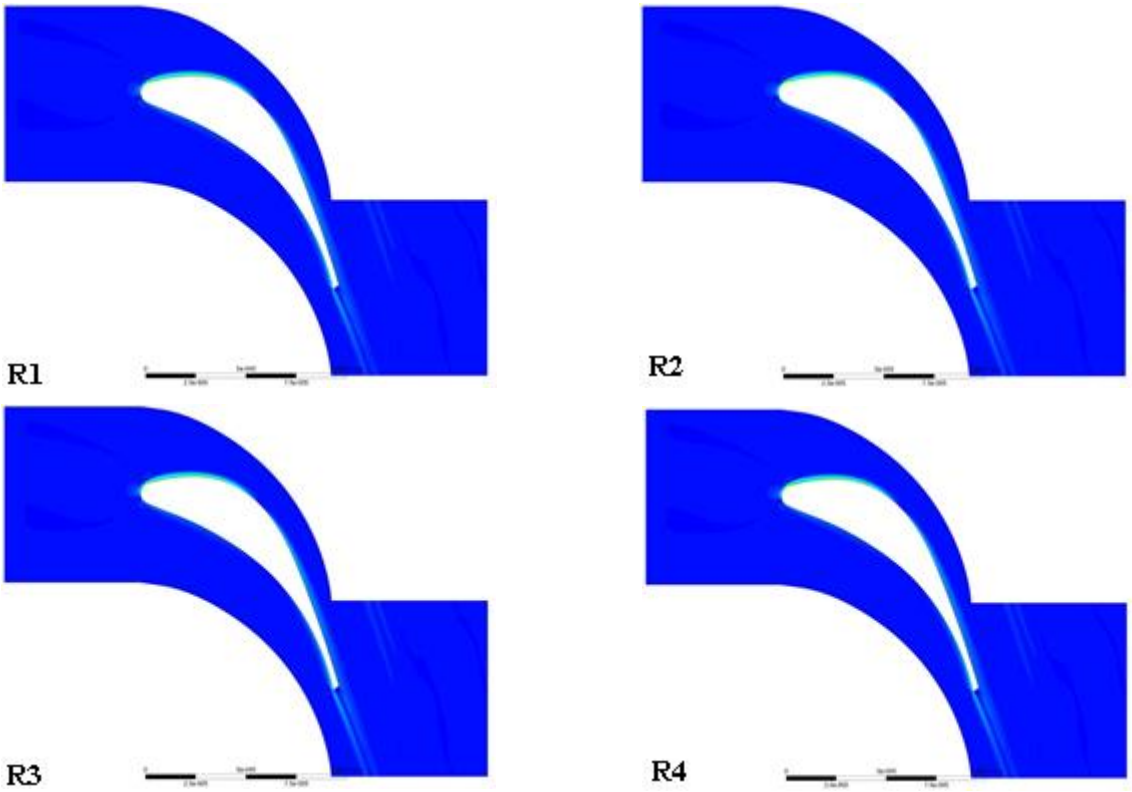

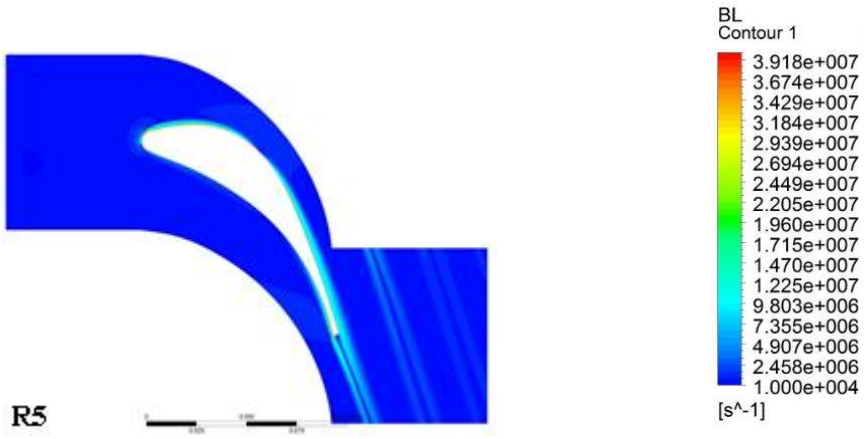

Figure 24: BL contours of the flow

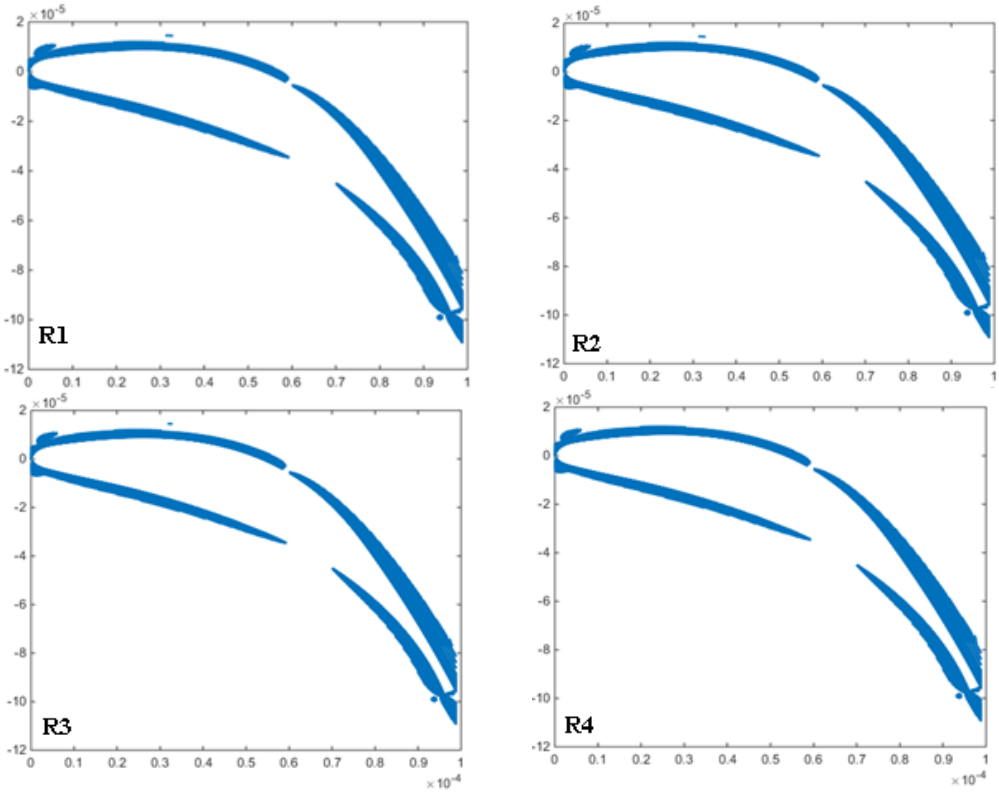

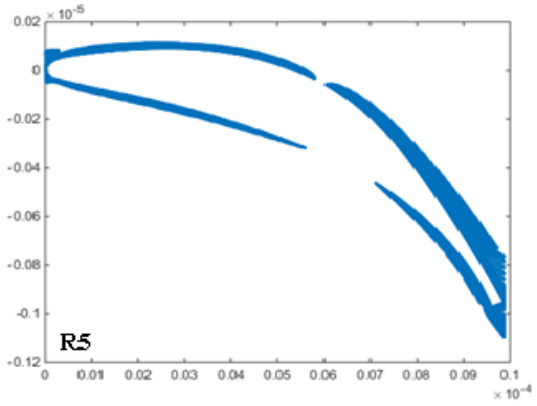

Figure 25: Boundary Layer after post processing

The presence of wide gaps in the boundary layer made it inaccurate conceptually and therefore to get more accurate boundary layer the second method was adopted.

The calculation of boundary layer was based on the principle of vorticity. The vorticity remains non zero within the boundary layer. Outside the boundary layer the flow is inviscid and irrotational because of the fact, the effect of viscosity is limited within the boundary layer **[29]**. Therefore, flow outside the boundary layer remains potential flow at any instant of time as well as with the change in velocity through the blade. The concept can be understood with some mathematical derivation as described **[30]**.

Taking the curl of the Navier-Stokes equation:

$$\boldsymbol{\nabla} X[\frac{\partial \boldsymbol{u}}{\partial t} + (\boldsymbol{u}.\boldsymbol{\nabla})\boldsymbol{u} = -\frac{1}{\rho}\boldsymbol{\nabla} p + \nu\Delta\boldsymbol{u}]$$

Applying vector mathematics:

$$\boldsymbol{\nabla} X(\boldsymbol{u}.\boldsymbol{\nabla})\boldsymbol{u} = \boldsymbol{u}.\boldsymbol{\nabla}(\boldsymbol{u} X\boldsymbol{\nabla}) - [(\boldsymbol{\nabla} X\boldsymbol{u}).\boldsymbol{\nabla}]\boldsymbol{u} + \boldsymbol{\nabla}.\boldsymbol{u}\boldsymbol{\nabla} X\boldsymbol{u}$$

Also, $\boldsymbol{\omega} = \boldsymbol{\nabla} X\boldsymbol{u}$

$$\boldsymbol{\nabla} X(\boldsymbol{u}.\boldsymbol{\nabla})\boldsymbol{u} = (\boldsymbol{u}.\boldsymbol{\nabla})\boldsymbol{\omega} - (\boldsymbol{\omega}.\boldsymbol{\nabla})\boldsymbol{u}$$

Since, $\boldsymbol{\nabla} X\boldsymbol{\nabla}\boldsymbol{p} = 0$ and $\boldsymbol{\nabla}.\boldsymbol{u} = 0$

Substituting the above conditions

$$\frac{D\boldsymbol{\omega}}{Dt} = (\omega.\boldsymbol{\nabla})\boldsymbol{u} + \nu\Delta\boldsymbol{\omega}$$

The first term in the right hand side describes the effect of velocity variation on the vorticity which is vorticity twisting and stretching in three dimension. Whereas the second term indicates the influence of viscosity in the production of vorticity down a vorticity gradient.

During steady state condition the left hand side of the equation becomes zero. The equation transforms into the following form.

$(\omega.\boldsymbol{\nabla})\boldsymbol{u} + \nu\Delta\boldsymbol{\omega} = 0$

Therefore, the production of vorticity within the boundary layer the combination of the velocity and fluid viscosity whereas as outside the boundary layer it is zero.

Applying the same concept in CFD Post and obtaining the coordinates of iso-surface at 0.99 ratio, the outer edge of the boundary layer can be determined. The boundary layer is depicted in figure 26.

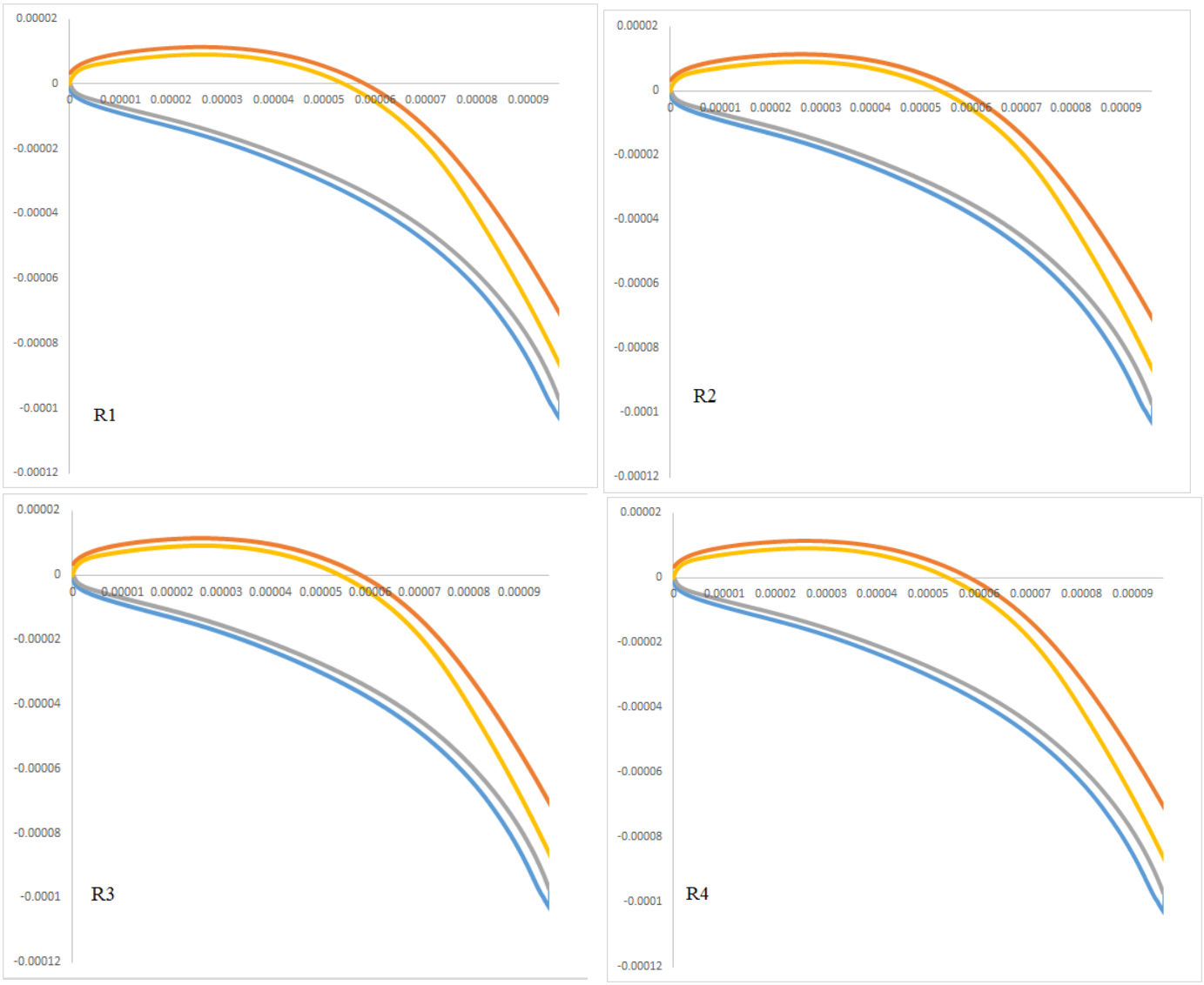

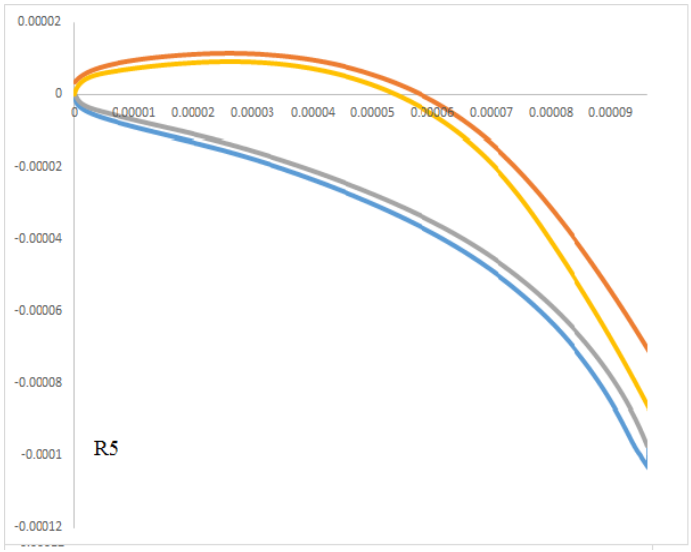

Figure 26: Boundary Layer on the Blade

In figure 27 the plots for friction velocity verses fraction of surface distance is graphed. From the plots it can be noticed that friction velocity for all simulations with different droplet size is same. The friction velocity is an important parameter to determine the zone of diffusional deposition as indicated in equation 3.5 and 3.7.

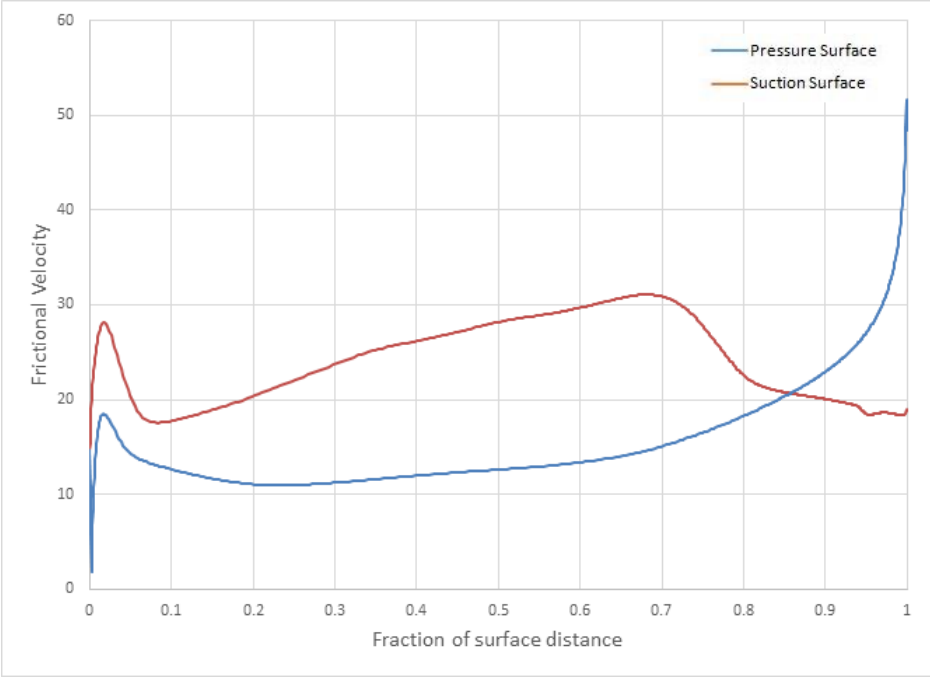

Figure 27: Friction Velocity

The effect of surface roughness for all the simulation is considered to have negligible influence mainly because of two reasons. The first reason being the laminar zone where τ_+ is very small which is dominated by turbulent-particle diffusion mechanism is only nearly 10% of total true chord. The second reason is that when τ_+ gradually increases or more precisely $\tau_+ < 2$, the effect of surface roughness has negligible influence on deposition.

The theoretical prediction of diffusional deposition is described in terms of F_D known as fractional diffusional deposition rate is very well described in reference **[25]** as "Considering the mass flow rate of water entering the blade row through a stream tube of thickness dR situated at a radial distance R from the turbine axis at blade inlet, F_D is defined as the fraction of water flow rate which is deposited on the blade by diffusional deposition."

In case of diffusional mechanism of steam turbine, the most dominant regime being eddy diffusion-impaction regime and partially particle-inertia moderated regime. The diffusional mass transfer is highest in eddy diffusion-impaction regime whereas the deposition of mass starts declining as the regime of deposition transfer from eddy-diffusion to inertia-moderated. In eddy-diffusion regime where $0.1 < \tau_+ < 10$ the deposition occurs due to particle transportation to the surface by intermittent turbulent bursts of fluid which disrupts the sublayer. Whereas for large particle $\tau_+ < 10$, the deposition is small due to damping effect of turbulent eddies.

The values of fractional diffusional deposition cannot be directly obtained from the software. Therefore, a number of new variables were introduced in CFD Post to obtain depositional velocity. For obtaining the deposition, another important parameter is droplet concentration at the edge of boundary layer. The edge of boundary layer was obtained by making isosurface in CFD Post as shown in figure 26. Then with bit of calculation Excel the fractional diffusional deposition was calculated. The detail of the process and variables are indicated in Appendix 2.

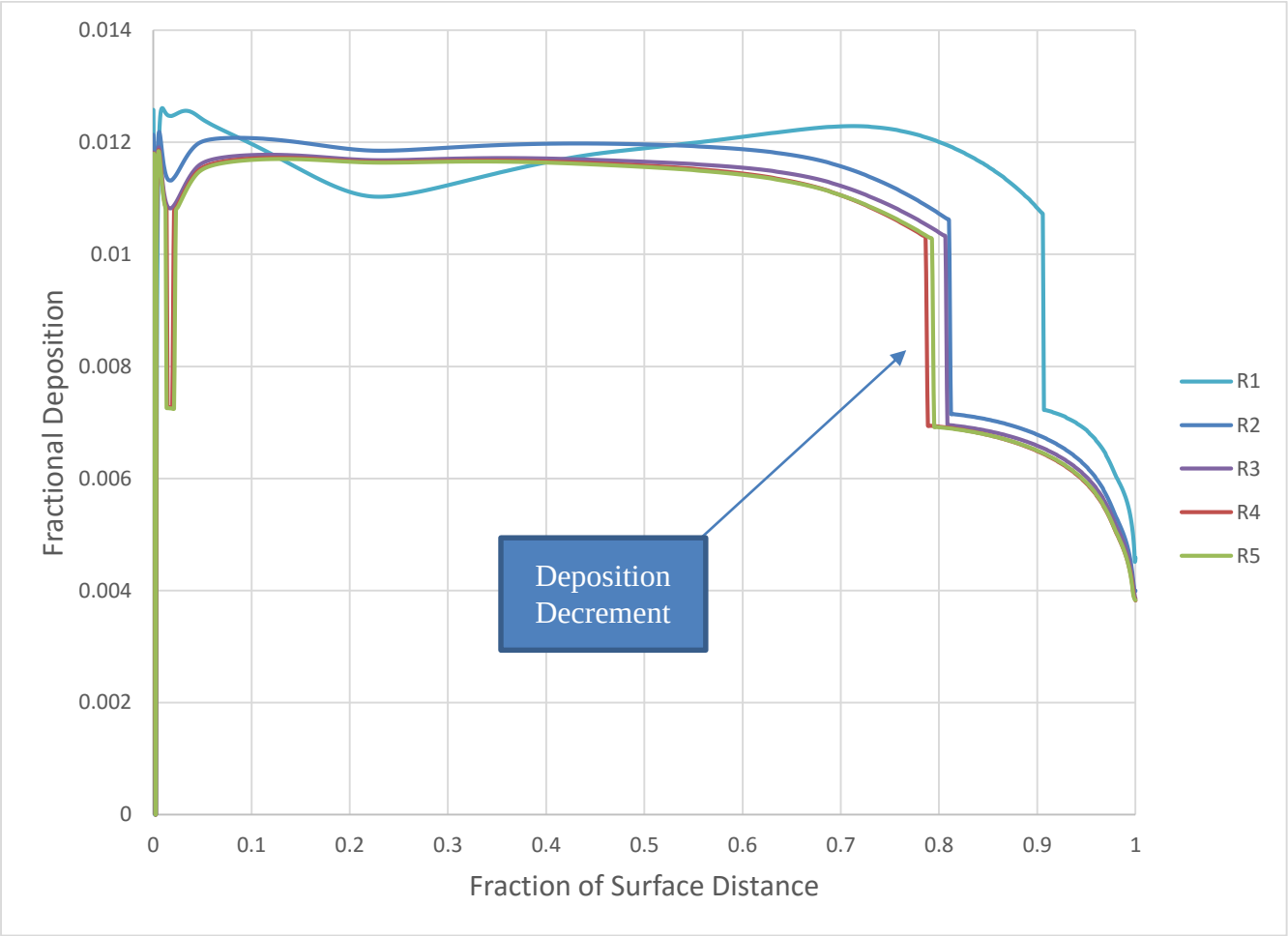

Figure 28: Fractional Diffusional Deposition on Pressure Surface

In figure 28 and 29 plots the graph of fractional diffusional deposition for pressure surface and suction surface respectively. The deposition is maximum for the droplet with minimum size and gradually decreases as the size increases. It is also noticeable as the droplet size is increased the deposition after a certain droplet size do not show considerable change. The deposition near the trailing edge of pressure surface and nearly after 25% of blade surface distance from leading edge for suction surface as shown in figures 28 and 29, suddenly decreases due to the change of regime from eddy-diffusion to inertia-moderated. Another interesting fact is that suction surface attains the transition of regime much earlier as compared to pressure surface.

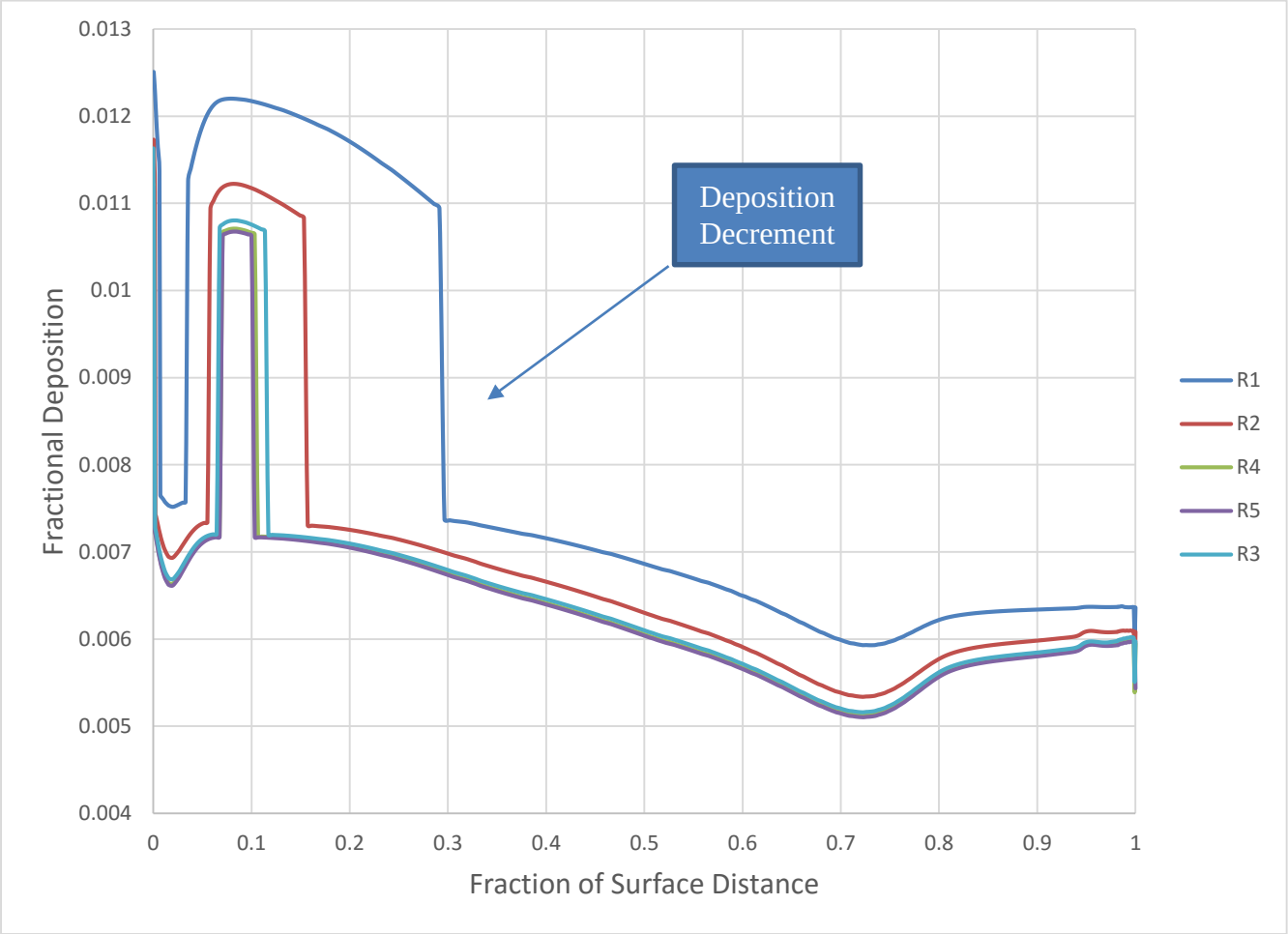

Figure 29: Fractional Diffusional Deposition on Suction Surface

6.5 Inertial Deposition

The inertial deposition can best be visualized physically by observing the streamlines of water droplets. Droplets of considerable size cannot follow the stream lines of the vapor due to its inertia and unable to follow highly curved path within the turbine blades and they graze the surface of the blade. When the streamline of a droplet grazes the blade surface, then there is the maximum probability of having deposition and maximum grazing happens near the trailing edge in both pressure surface and suction surface. At the leading edge near the stagnation point the stream lines are highly curved and lies a great chance that droplets of high inertia get detached from vapor steam line and may cause deposition.

The droplet size is a dominant factor for inertial deposition along with blade geometry. For simple blade profiles deposition is almost constant though out the surface distance but for the blade profile of high curvature the deposition varies a lot through the surface distance. The droplets having greater size are

having greater inertial effect, therefore it is expected that droplet with highest radius shall give highest deposition.

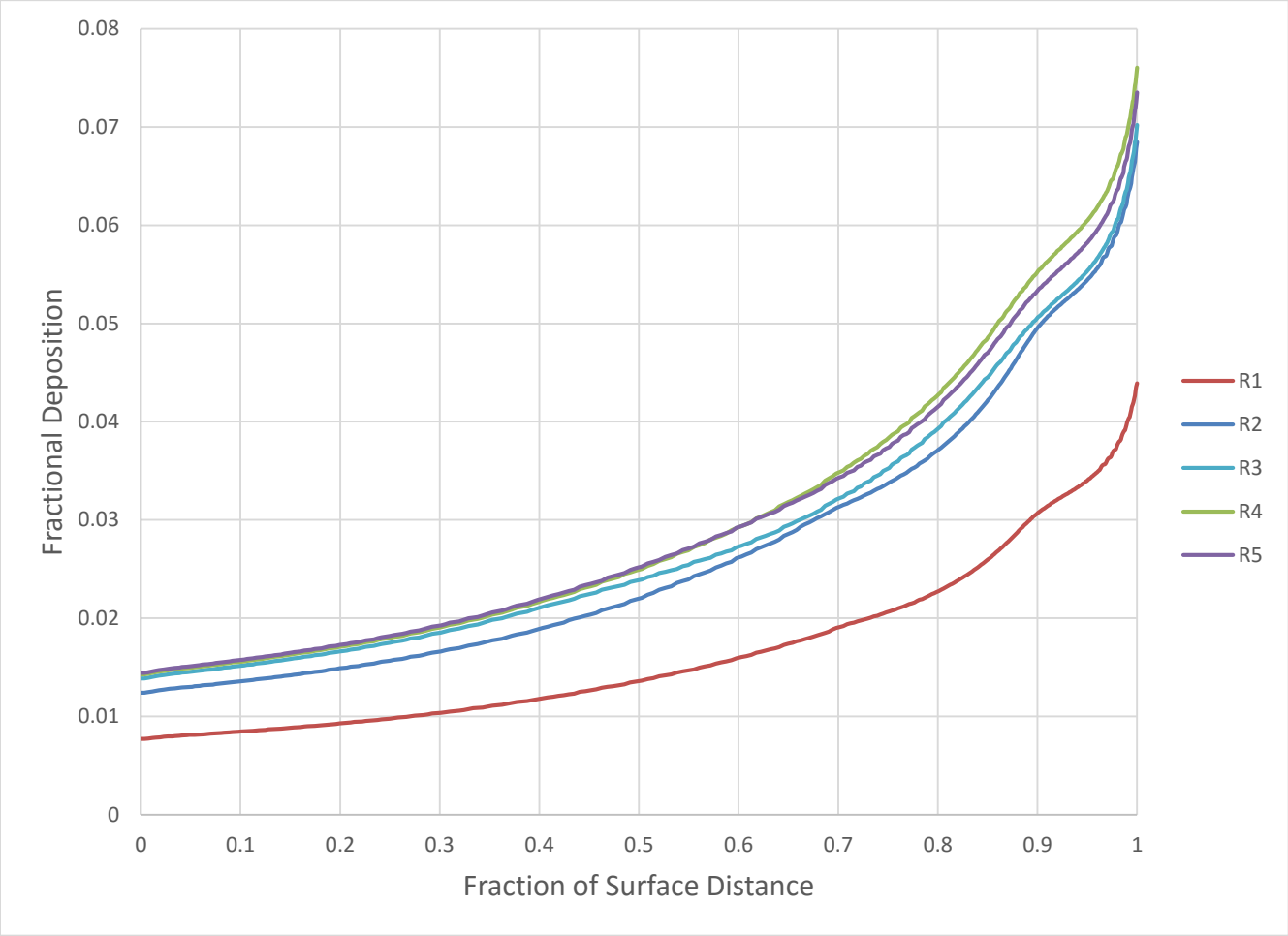

Figure 30: Fractional Inertial Deposition on Pressure Surface

Description of inertial deposition can be given by a factor known as fractional inertial deposition F_I obtained from equation 3.26 can be defined as the fraction of water flow rate deposited on the surface of the blade. In figure 30 and 31 fractional inertial deposition for pressure surface and suction surface is shown respectively. The results matches satisfactorily with expectation, as the droplet size is increased the deposition also gets increased. The deposition is increased more towards trailing edge for both pressure surface and suction surface. One very noteworthy and interesting fact is that deposition rate do not vary a lot after a certain size of droplet, for example after R4 there is not much considerable change in deposition in both the surfaces of the blade profile.

The post processing required for inertial deposition was much less and less complex as compared to diffusional deposition. The process was rather direct and straight forward and shown in Appendix 3.

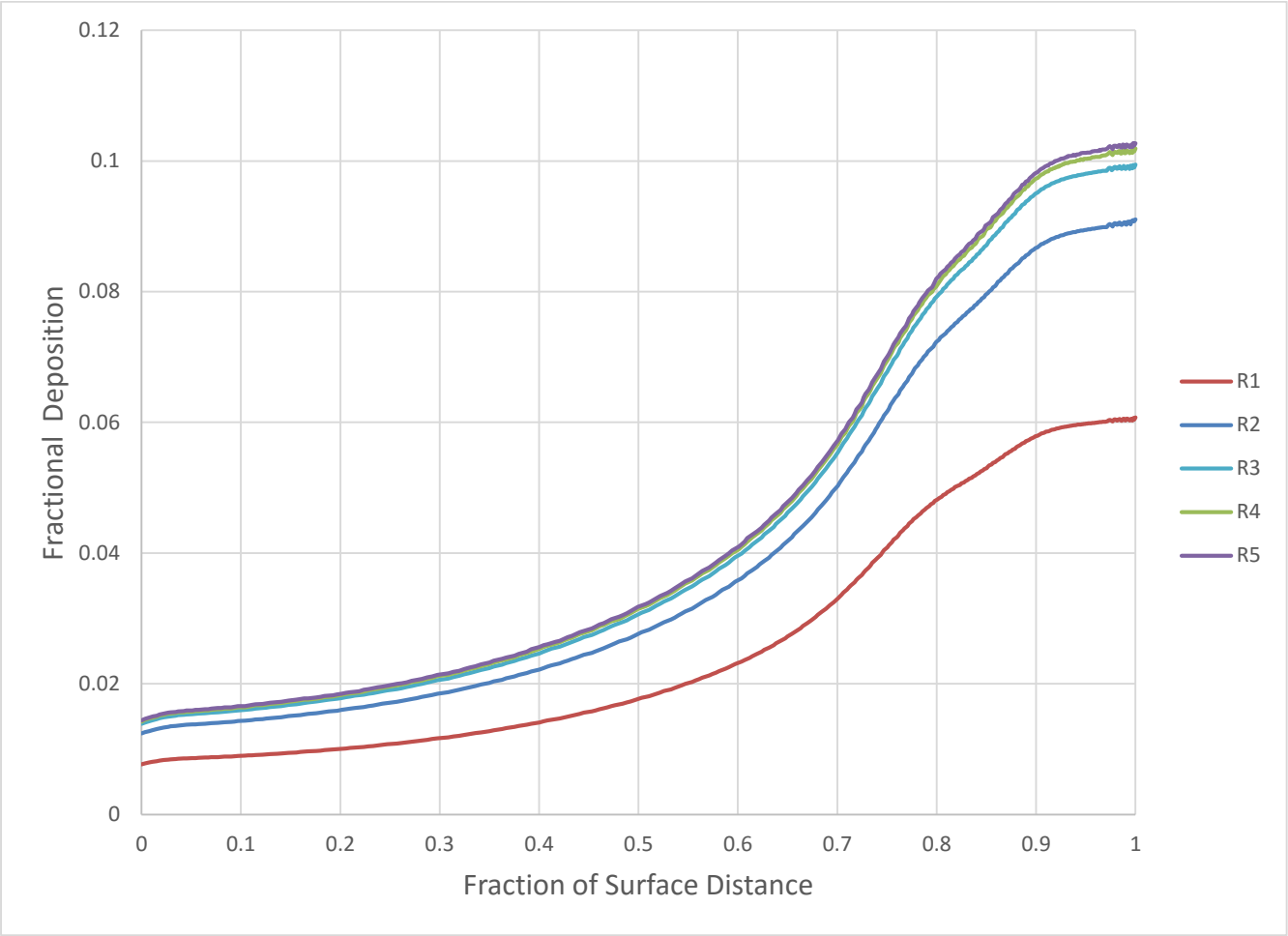

Figure 31: Fractional Inertial Deposition on Suction Surface

6.6 Total Deposition

Total deposition on the blade surface is the summation of fraction diffusional deposition and inertial deposition.

$F_T = F_D + F_I$

Figure 32 and 33 shows the plots for total deposition for pressure surface and suction surface respectively. In the trailing edge the deposition is quite high as the deposition is mostly dominated by inertial deposition. The size of the droplet has a pronounced influence on the deposition phenomenon. Generally, as the radius of the droplets increases the deposition is increased for the droplets ranging in size of 0.4µm to 1µm. A very interesting fact in both figure 32 and 33 is that deposition R4 is greater than deposition R5 except near the trailing edge. This is due to the fact that for R5 the diffusional deposition becomes

negligible as the size of the droplet is quite high of about 1.2µm. In this range of size the diffusional deposition is almost absent as also seen from plots for diffusional deposition.

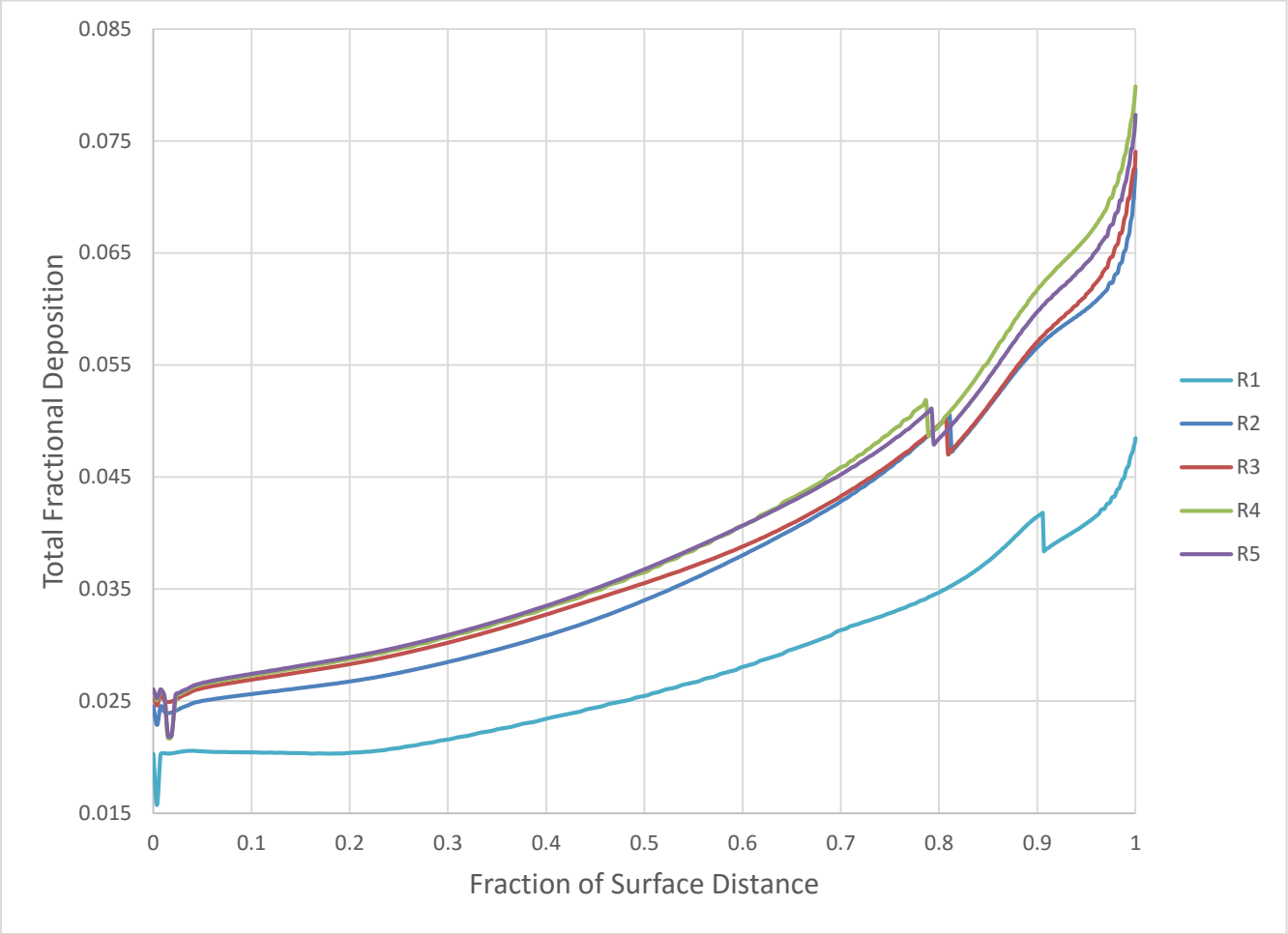

Figure 32: Total Deposition on Pressure Surface

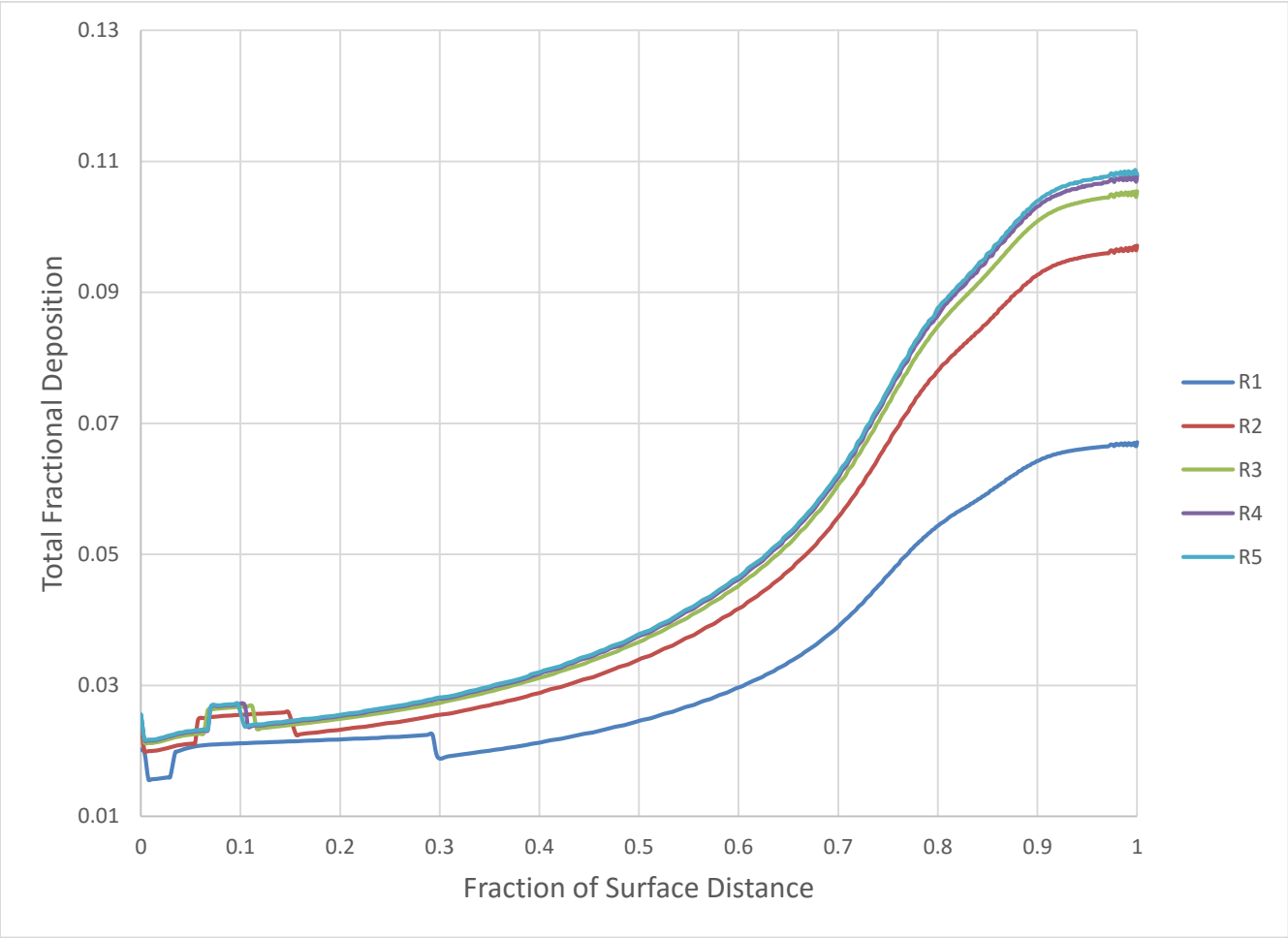

Figure 33: Total Deposition on Suction Surface

7. Conclusion

The long existing challenge in steam turbine that is droplet deposition which is also responsible for the erosion of penultimate and ultimate stages of blade rows. The thesis aims to study the deposition phenomenon for the droplet size range of 0.4µm to 1.2µm on a last stage stator blade of a 660 MW steam turbine. The droplets of various size within the above size range keeping the other boundary conditions to be the same were used for the simulation. The mesh in the computational domain was totally structured type with a very high mesh density near the wall of the blade. The mesh quality plays a crucial role due to the complexity of the physics in the simulation.

Two different kinds of deposition phenomenon was studied in the work namely diffusional deposition and inertial deposition. Boundary layer plays a significant role in diffusional deposition. As diffusional deposition is a boundary layer phenomenon caused due to various reasons such as combined effect of

Brownian and eddy diffusion, turbulent bursts of fluid disrupting the sublayer, therefore the boundary layer development is quite sensitive to droplet size. The turbine works mainly eddy diffusion impaction regime where the deposition velocity changes quite abruptly with respect to dimensionless relaxation time. The eddy diffusion impaction regime occurs in turbulent boundary layer. Therefore, accurate prediction of laminar-turbulent transition along with boundary layer is vital. Unlike in turbulent boundary layer, the deposition in laminar boundary layer that is in turbulent particle diffusion regime is quite small or negligible. The maximum fractional diffusional deposition on both pressure side and suction side is comparable although total deposition in pressure side is greater than that of suction side. It is also observed that the diffusional deposition is maximum in smaller size droplets. There is a remarkable decrement in deposition from 0.4μm to 0.8μm droplet size and after 1μm there is no appreciable change in deposition. The results of simulation matches well with established theory as indicated in figure 6, where diffusional deposition for larger droplets in Particle Inertia- Moderated Regime not only saturates but also degrades. As diffusional deposition is associated with boundary layer, the smaller size droplet can well interact with boundary layer and cause deposition whereas the deposition for considerably larger droplets falls in particle inertia moderated regime where the droplet inertia damps the effect of turbulent eddies which decreases the diffusional deposition.

The inertial deposition becomes quite dominant when the droplet size increases. Due to the inertial of the larger droplets, they cannot follow the stream lines of the steam in highly curved flow direction. The droplets detach themselves from steam stream line and deposit themselves on the surface of blade. The deposition is increased as the droplet size is increased. Although after 1μm of droplet size the deposition rate have no remarkable increment. The deposition is maximum in the trailing edge for both pressure side and suction side. Although the total deposition in suction side is greater than that of pressure side with a maximum deposition of 10% just in the vicinity of trailing edge, whereas maximum deposition in pressure surface is about 7.5%. The shape of the blade plays an important role in inertial deposition as well.

The inertial deposition is dominant for the chosen range of droplet size in maximum region of the turbine blade. Therefore, the total deposition increases as the droplet size is increased except for 1.2μm droplet group. Here, the diffusional deposition becomes almost negligible due large droplet diameter and the total deposition decreases than that of the 1μm droplet group. The pressure side and suction side experience the same kind of phenomenon.

Further work can be done extensively on the part load working condition of the turbine and then designing the turbine in such a way to have minimum effect of depositional erosions. Detailed study can be made with three dimensional calculations as the shape of the blade change extensively in radial as well as axial directions which leads to secondary vortices and effect of three dimensionalities on boundary layer and droplet trajectory which eventually responsible for deposition.

Appendix 1

The equilibrium simulation was performed at first and then using the result of equilibrium simulation, non-equilibrium simulations were performed for different droplet radius.

The prediction of the edge of the boundary layer was an important step for calculation of diffusional deposition. The geometry of blade profile was quite complex to be able to locate boundary layer over it directly or by any simple means. To locate boundary layer over the blade surface a new formula is introduced as:

$$BL = \left(\frac{\partial u}{\partial x} + \frac{\partial v}{\partial x} + \frac{\partial w}{\partial x}\right)\hat{\imath} + \left(\frac{\partial u}{\partial y} + \frac{\partial v}{\partial y} + \frac{\partial w}{\partial y}\right)\hat{\jmath} + \left(\frac{\partial u}{\partial z} + \frac{\partial v}{\partial z} + \frac{\partial w}{\partial z}\right)\hat{k}$$

The formula relies on the fact of velocity gradient and boundary layer has very strong existence of velocity gradient from wall to mean flow. Although flow inside the turbomachinery is quite notorious but still the above formula give quite good result in prediction of boundary layer.

In CFD-Post BL was introduced as a variable and contours were plotted. The results of the contours were shown in figure 24. Once again the figure is given here to maintain the continuity.

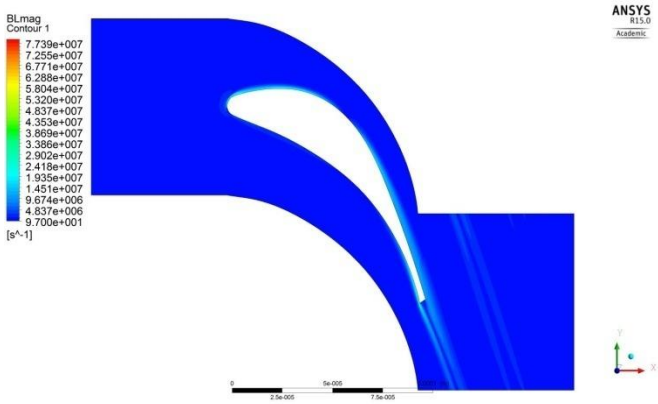

Then, all the values of BL were exported to excel for further post processing. As the whole domain contains innumerable points little processing was done in MS Excel and then it was taken to MATLAB. The formation of boundary layer will only be near the blades and with the use of few conditional statements the calculation points were reduced in Excel. In the last column '1' indicates the desired data that should considered whereas '0' are not to be considered.

4	[Data]							
5	X[m]	Y[m]	Z[m]	BL[s^-1]				
6	3.30E-05	1.15E-05	0.00E+00	7.33E+05	1	1	0	0
7	3.29E-05	1.10E-05	0.00E+00	1.46E+06	1	1	1	1
8	3.23E-05	1.11E-05	0.00E+00	1.48E+06	1	1	1	1
9	3.24E-05	1.15E-05	0.00E+00	7.51E+05	1	1	0	0
10	3.25E-05	1.19E-05	0.00E+00	7.06E+04	1	1	0	0
11	3.31E-05	1.19E-05	0.00E+00	6.28E+04	1	1	0	0
12	3.34E-05	1.14E-05	0.00E+00	7.21E+05	1	1	0	0
13	3.33E-05	1.10E-05	0.00E+00	1.44E+06	1	1	1	1
14	3.35E-05	1.18E-05	0.00E+00	6.20E+04	1	1	0	0
15	3.17E-05	1.12E-05	0.00E+00	1.51E+06	1	1	1	1
16	3.18E-05	1.16E-05	0.00E+00	7.72E+05	1	1	0	0
17	3.19E-05	1.20E-05	0.00E+00	7.88E+04	1	1	0	0
18	3.23E-05	1.09E-05	0.00E+00	2.49E+06	1	1	1	1
19	3.28E-05	1.09E-05	0.00E+00	2.46E+06	1	1	1	1
20	3.17E-05	1.10E-05	0.00E+00	2.52E+06	1	1	1	1
21	3.33E-05	1.08E-05	0.00E+00	2.44E+06	1	1	1	1
22	3.26E-05	1.24E-05	0.00E+00	3.66E+05	1	1	0	0
23	3.32E-05	1.23E-05	0.00E+00	3.78E+05	1	1	0	0
24	3.36E-05	1.22E-05	0.00E+00	3.71E+05	1	1	0	0
25	3.20E-05	1.24E-05	0.00E+00	3.55E+05	1	1	0	0
26	3.27E-05	1.28E-05	0.00E+00	5.91E+05	1	1	0	0
27	3.33E-05	1.27E-05	0.00E+00	5.97E+05	1	1	0	0
28	3.37E-05	1.26E-05	0.00E+00	5.94E+05	1	1	0	0
29	3.22E-05	1.28E-05	0.00E+00	5.85E+05	1	1	0	0
30	3.28E-05	1.32E-05	0.00E+00	7.23E+05	1	1	0	0
31	3.34E-05	1.31E-05	0.00E+00	7.26E+05	1	1	0	0
32	3.39E-05	1.30E-05	0.00E+00	7.22E+05	1	1	0	0
33	3.23E-05	1.32E-05	0.00E+00	7.19E+05	1	1	0	0
34	3.30E-05	1.36E-05	0.00E+00	7.91E+05	1	1	0	0
35	3.35E-05	1.35E-05	0.00E+00	7.91E+05	1	1	0	0
36	3.40E-05	1.34E-05	0.00E+00	7.88E+05	1	1	0	0
37	3.24E-05	1.36E-05	0.00E+00	7.90E+05	1	1	0	0
38	3.31E-05	1.40E-05	0.00E+00	8.18E+05	1	1	0	0
39	3.37E-05	1.39E-05	0.00E+00	8.17E+05	1	1	0	0

Then after Excel operation is over the data was loaded in MATAB.

The MATLAB code for obtaining boundary layer around the blade is as follows:

```
clear all
close all
clc

load export_Copy_1.txt
plot(export_Copy_1(:,1),export_Copy_1(:,2),'.')


% data_1=[export_Copy_1(:,4) export_Copy_1(:,1:3)];
%
% data_2=sort(data_1);
% data_3=data_2(115723:end,:);

A=find(export_Copy_1(:,4)>0.5);
data_4=export_Copy_1(A,:);
data_4=sortrows([data_4(:,2) data_4(:,1) data_4(:,3:4)])
%data_3-data_4

figure(1)
plot(data_4(:,2),data_4(:,1),'.')
hold on

figure(2)
plot3(data_4(:,2),data_4(:,1),data_4(:,3),'.')

    distf=find(sqrt((data_4(2:end,1)-data_4(1:end-1,1)).^2+(data_4(2:end,2)-
data_4(1:end-1,2)).^2)>0.001);
%figure(1)
   % plot(data_4(distf+1,1),data_4(distf+1,2),'c.')

   hold on
%1626468
```

```
B=find(data_4(:,3)<constant);
data_5=data_4(B,:);
plot(data_5(:,2),data_5(:,1),'r.-')

 hold off

 figure (3)
 %data_5=sort(data_5)
 plot(data_5(:,2),data_5(:,1),'r.','LineWidth',1.5)

 handle=gca;
set(handle,'LineWidth',1,'fontsize',16,'FontName','Times New Roman')
%set(handle,'Position',[0.07 0.16 0.41 0.75])
 %set(handle,'XTick',[0:0.25:2])
 %set(handle,'XTickLabel',[0:0.25:2])
 set(gcf, 'PaperPosition', [0 0 20 10]); %Position plot at left hand corner with
width 5 and height 5.
 set(gcf, 'PaperSize', [20 10]); %Set the paper to have width 5 and height 5.
 saveas(handle, 'my_curve', 'tiff') %Save figure


 AA=[data_5(:,2) data_5(:,1) zeros(length(data_5(:,1)),1)];
 %save (myLine,data_5(:,1),'data_5(:,2)')
 save my_line.txt AA -ASCII
```

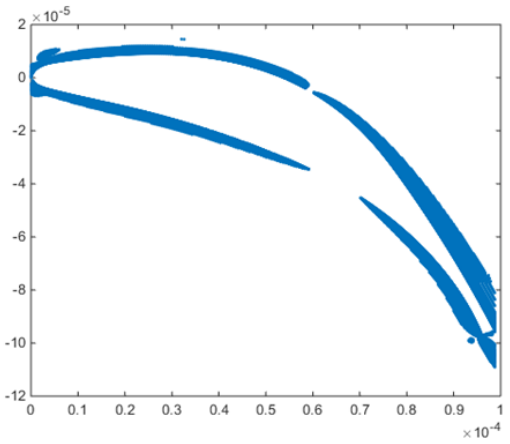

After post processing in MATLAB the plot of boundary layer was obtained as was shown in figure 25 The same figure is shown here as well. The figure describes the position of boundary layer. There are two places of discontinuity where boundary layer is absent. Although in reality the boundary layer is not absent but as the formula relies on velocity gradient and here in these two position velocity gradient is very small though present. So, to make the result practically viable the boundary layer in these two positions are extrapolated from its side. Then the coordinate of the outer edge is collected by means of a digital software and then exported to CFD-Post as polylines.

The formula was tested by two ways. A new variable known as BLmag was introduced in CFD Post and same process as above was repeated, then it was found the prediction of boundary layer is very nearly the same. Secondly, few perpendiculars were drawn on blade surface in CFD-Post as lines. Then velocity profile on these lines were observed. Then the coordinates were noted where velocity change is almost

zero or relative very small and then the coordinates were matched with figure 25 and was found satisfactory.

Appendix 2

Some of the variables those were used for post processing are as follows in the purpose of example:

CE=(-0.0002*(Stk^2))+(0.0238*(Stk))+0.3962

D=boltzmann*H2Og.Temperature*(1+2.7*Kn)/(3*3.14*H2Ol.Particle Diameter*H2Og.Dynamic Viscosity)

Deposition Velocity=Vp*fv

IB=if(xx>5,5*loge(25.2/abs(sp+rp-4.8)),24.5)

IBdeno=5*loge(25/(sp+rp-4.8))

IS=if(xx<5,14.5*(Sc^2/3)*(fphi+gphi-fphi1-gphi1),0)

Kn=MFP/H2Ol.Particle Diameter

MFP=boltzmann*H2Og.Temperature/(1.414*3.14*Total Pressure*Vapordia*Vapordia)

Pitch =87.59e-3 [m]

Sc=neug/D

Stk=tau/(2*LERadius)

Vp=(IS+IB)^-1

a=14.5*(Sc^(-1/3))

fphi=(loge(((1+phi)^2)/(1-phi+phi^2)))/6

fphi1=(loge(((1+phi1)^2)/(1-phi1+phi1^2)))/6

fv=(H2Og.Wall Shear/H2Og.Density)^0.5

gphi=(atan((2*phi-1)/(3^0.5)))/(3^0.5)

gphi1=(atan((2*phi1-1)/(3^0.5)))/(3^0.5)

neug=H2Og.Dynamic Viscosity/H2Og.Density

phi=5/a

phi1=(sp+rp)/a

rp=(H2Ol.Particle Diameter/2)*fv/neug

sp=0.69*taup

tau=(H2Ol.Particle Diameter^2)*H2Ol.Density*(1+2.7*Kn)/(18*H2Og.Dynamic Viscosity)

taup=(H2Ol.Particle Diameter^2)*H2Ol.Density*(1+2.7*Kn)/(18*H2Og.Dynamic Viscosity)

xx=sp+rp

Then they were further calculated in excel to get the final result.

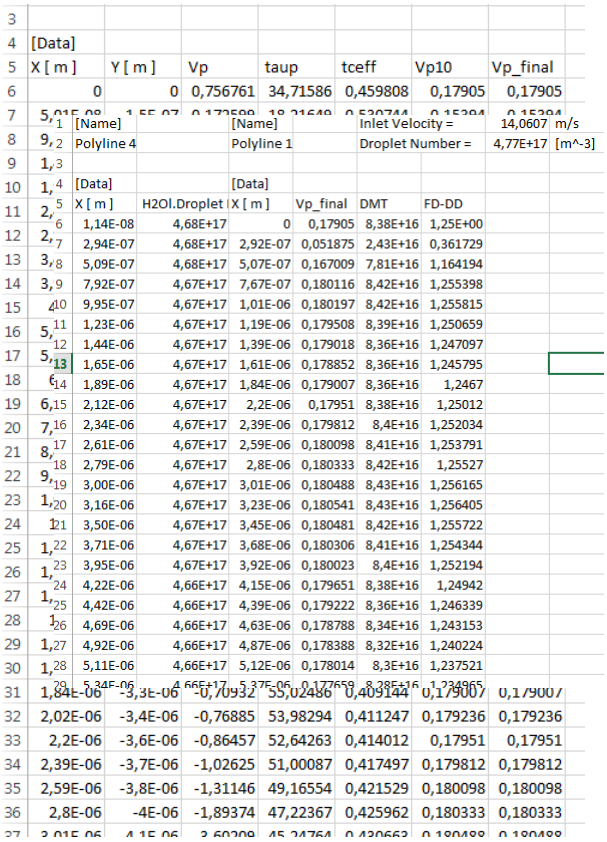

[Data]							
X [m]	Y [m]	Vp	taup	tceff	Vp10	Vp_final	
0	0	0,756761	34,71586	0,459808	0,17905	0,17905	
5,01E-08	1,55E-07	0,172599	18,21649	0,530744	0,15294	0,15294	
[Name]			[Name]		Inlet Velocity =	14,0607	m/s
Polyline 4			Polyline 1		Droplet Number =	4,77E+17	[m^-3]
[Data]			[Data]				
X [m]	H2Ol.Droplet		X [m]	Vp_final	DMT	FD-DD	
1,14E-08	4,68E+17		0	0,17905	8,38E+16	1,25E+00	
2,94E-07	4,68E+17		2,92E-07	0,051875	2,43E+16	0,361729	
5,09E-07	4,68E+17		5,07E-07	0,167009	7,81E+16	1,164194	
7,92E-07	4,67E+17		7,67E-07	0,180116	8,42E+16	1,255398	
9,95E-07	4,67E+17		1,01E-06	0,180197	8,42E+16	1,255815	
1,23E-06	4,67E+17		1,19E-06	0,179508	8,39E+16	1,250659	
1,44E-06	4,67E+17		1,39E-06	0,179018	8,36E+16	1,247097	
1,65E-06	4,67E+17		1,61E-06	0,178852	8,36E+16	1,245795	
1,89E-06	4,67E+17		1,84E-06	0,179007	8,36E+16	1,2467	
2,12E-06	4,67E+17		2,2E-06	0,17951	8,38E+16	1,25012	
2,34E-06	4,67E+17		2,39E-06	0,179812	8,4E+16	1,252034	
2,61E-06	4,67E+17		2,59E-06	0,180098	8,41E+16	1,253791	
2,79E-06	4,67E+17		2,8E-06	0,180333	8,42E+16	1,25527	
3,00E-06	4,67E+17		3,01E-06	0,180488	8,43E+16	1,256165	
3,16E-06	4,67E+17		3,23E-06	0,180541	8,43E+16	1,256405	
3,50E-06	4,67E+17		3,45E-06	0,180481	8,42E+16	1,255722	
3,71E-06	4,67E+17		3,68E-06	0,180306	8,41E+16	1,254344	
3,95E-06	4,67E+17		3,92E-06	0,180023	8,4E+16	1,252194	
4,22E-06	4,66E+17		4,15E-06	0,179651	8,38E+16	1,24942	
4,42E-06	4,66E+17		4,39E-06	0,179222	8,36E+16	1,246339	
4,69E-06	4,66E+17		4,63E-06	0,178788	8,34E+16	1,243153	
4,92E-06	4,66E+17		4,87E-06	0,178388	8,32E+16	1,240224	
5,11E-06	4,66E+17		5,12E-06	0,178014	8,3E+16	1,237521	
5,34E-06	4,66E+17		5,37E-06	0,177659	8,28E+16	1,234965	
1,84E-06	-3,3E-06	-0,70932	55,02486	0,409144	0,179007	0,179007	
2,02E-06	-3,4E-06	-0,76885	53,98294	0,411247	0,179236	0,179236	
2,2E-06	-3,6E-06	-0,86457	52,64263	0,414012	0,17951	0,17951	
2,39E-06	-3,7E-06	-1,02625	51,00087	0,417497	0,179812	0,179812	
2,59E-06	-3,8E-06	-1,31146	49,16554	0,421529	0,180098	0,180098	
2,8E-06	-4E-06	-1,89374	47,22367	0,425962	0,180333	0,180333	
3,01E-06	4,15E-06	3,60209	45,24764	0,430663	0,180488	0,180488	

For diffusional deposition, the dimensionless diffusional deposition velocity is calculated.

And polyline 4 indicates the droplet concentration at the edge of boundary layer. Then the coordinates of dimensionless diffusional deposition velocity and droplet concentration were matched and fractional diffusional deposition was calculated.

Appendix 3

Similarly the deposition for inertial deposition was calculated with excel.

1	[Name]			[Name]		R	6				
2	Polyline 1			Polyline 3		P	87,59				
3						s	97,2				
4	[Data]			[Data]							
5	X [m]	Y [m]	Stk	X [m]	Y [m]	H2Og.Velocity [m s^-1]	Stk_final	CE	FI_LE	FI_PS	FI_total
6	0	0	0,000205	0	4,38E-05	17,0207424	0,003482	0	0	0,007702	0,007702
7	3,43E-07	-1E-06	0,000204	3,49E-07	4,37E-05	17,0455246	0,003485	0	0	0,007707	0,007707
8	6,97E-07	-1,9E-06	0,000205	7,01E-07	4,37E-05	17,0680885	0,0035	0	0	0,007742	0,007742
9	1,1E-06	-2,5E-06	0,000206	1,06E-06	4,36E-05	17,1032448	0,003525	0	0	0,007797	0,007797
10	1,39E-06	-2,9E-06	0,000207	1,42E-06	4,36E-05	17,1275845	0,003542	0	0	0,007833	0,007833
11	1,84E-06	-3,3E-06	0,000208	1,78E-06	4,35E-05	17,1620502	0,003563	0	0	0,00788	0,00788
12	2,2E-06	-3,6E-06	0,000208	2,14E-06	4,35E-05	17,1969986	0,003578	0	0	0,007913	0,007913
13	2,59E-06	-3,8E-06	0,000208	2,51E-06	4,34E-05	17,2351685	0,003592	0	0	0,007944	0,007944
14	3,01E-06	-4,1E-06	0,000209	2,88E-06	4,34E-05	17,2751579	0,003606	0	0	0,007974	0,007974
15	3,23E-06	-4,2E-06	0,000209	3,26E-06	4,33E-05	17,3191357	0,003617	0	0	0,007998	0,007998
16	3,68E-06	-4,4E-06	0,000209	3,64E-06	4,33E-05	17,3665714	0,00363	0	0	0,008027	0,008027
17	3,92E-06	-4,5E-06	0,000209	4,02E-06	4,32E-05	17,4141121	0,003641	0	0	0,008052	0,008052
18	4,39E-06	-4,7E-06	0,000209	4,4E-06	4,32E-05	17,4596405	0,003653	0	0	0,008077	0,008077
19	4,63E-06	-4,9E-06	0,000209	4,79E-06	4,31E-05	17,5072937	0,003664	0	0	0,008101	0,008101
20	5,12E-06	-5,1E-06	0,000209	5,18E-06	4,31E-05	17,5584736	0,003676	0	0	0,008129	0,008129
21	5,61E-06	-5,3E-06	0,000209	5,58E-06	4,3E-05	17,6122608	0,003689	0	0	0,008157	0,008157
22	6,12E-06	-5,5E-06	0,00021	5,98E-06	4,3E-05	17,6671124	0,003702	0	0	0,008186	0,008186
23	6,37E-06	-5,6E-06	0,00021	6,38E-06	4,29E-05	17,7223778	0,003715	0	0	0,008214	0,008214
24	6,63E-06	-5,7E-06	0,00021	6,79E-06	4,29E-05	17,7798634	0,003727	0	0	0,008242	0,008242

References

1 **Crane, R.** Droplet deposition in steam turbines. *Proc. Inst. Mech. Eng. Part C* , 2004, **218**, 859-870.

2 **Bakhtar, F.,Ebrahimi, M., and Bamkole, B.**, 1995. "On the performance of a cascade of turbine rotor tip section blading in nucleating steam, part 2: wake traverses". Proc. Inst. Mech. Eng. Part C: J. Mech. Eng. Sci., Vol. 209, pp. 169– 177

3 **Bakhtar, F., Ebrahimi, M., and Webb, R.**, 1995. "On the performance of a cascade of turbine rotor tip section blading in nucleating steam, part 1: surface pressure distributions". Proc. Inst. Mech. Eng. Part C: J. Mech. Eng. Sci., Vol.209, pp. 115–124.

4 **White, A.J., Young, J.B., and Walters, P.T.**, 1996. "Experimental validation of condensing flow theory for a stationary cascade of steam turbine blade". Philos. Trans. Roy. Soc. Lond., Vol.A354, pp. 59–88.

5 **White, A. J., and Young, J. B.**, 1993. "Time-marching method for the prediction of two-dimensional unsteady flows of condensing steam". AIAA J. Propulsion and Power, Vol.9(4), pp. 579–587.

6 **Bakhtar, F., Mahpeykar, M. R.**, and Abbas, K. K., 1995. "An investigation of nucleating flows of steam in a cascade of turbine blading-theoretical treatment". ASME J. Fluids Eng., Vol.117, pp. 138–144.

7 **Gerber, A.G., and Kermani, M.J.**, 2004. "A pressure based Eulerian-Eulerian multi-phase model for non-equilibrium condensation in transonic steam flow". Int. J. Heat Mass Transfer,Vol.44, pp. 2217–2231.

8 **Senoo, S., and Shikano, Y.**, 2002. "Non-equilibrium homogeneously condensing flow analyses as design tools for steam turbines". In ASME FEDSM'02, Montreal, July 1418, FEDSM2002-31191.

9 **Starzmann, J., Kaluza, P.**, Casey, M. V., and Sieverding, F., 2013. "On kinematic relaxation and deposition of water droplets in the last stages of low pressure steam turbines". InProc.ASMETurboExpo, GT2013-95179, SanAntonio, Texas, USA, June 3-7, pp. 1-12.

10 **Friedlander, S. K., and Johnstone, H. F**., Deposition of suspended particles from turbulent gas streams, *Ind. Eng. Chem*., Vol. 49, 1957, 1151-1156

11 **Montgomery, T. L., and Corn, M**., Aerosol deposition in a pipe with turbulent airflow, *J. Aerosol Science*, Vol 40, 1970, 185-213

12 **Liu, B. Y. H., and Agarwal, J. K**., Experimental observation of aerosol deposition in turbulent flow, *J. Aerosol Science* , Vol.-5, 1974, 145-155

13 **Cleaver, J. W., and Yates, B**., A sub-layer model for the deposition of particles from a turbulent flow, Chem. Eng. Sci., Vol. 30, 1975, 983-992

14 **Reeks, M. W., and Skyrme, G.**, The dependence of particles deposition velocity on particles inertia in turbulent pipe flow, *J. Aerosol Science*, Vol. 7, 1976, 485-495

15 **El-Shobokshy, M. S., and Ismail, I. A.**, Deposition of aerosol particles from turbulent flow onto rough pipe wall, *Atmospheric Environment*, Vol. 14, 1980, 297-304

16 **Wood, N. B.**, A simple method for the calculation of turbulent deposition to smooth and rough surfaces, *J. Aerosol Science*, Vol 12, 1981, 257-290

17 **Parker, G. J., and Lee, P.**, Studies of the deposition of submicron particles on turbine blades, *Proc. Inst. Mech. Engnrs*, Vol. 186, 1972, 519-526

18 **Parker, G. J., and Ryley, D. J.**, Equipment and techniques for studying the deposition of submicron particles of turbine blades, *Proc. Inst. Mech. Engnrs.*, Vol. 184, Part 3C, 1969-70, 43-51.

19 **Gyarmathy, G.**, Bases of a Theory for Wet Steam Turbines, Bull. 6. Inst. for thermal turbomachines, Federal Technical University, Zurich, CEGB Translation T-781, 1962

20 **ANSYS**, ANSYS Fluent Theory Guide [Online], Chapter-18 page-40, Available:http://orange.engr.ucdavis.edu/Documentation12.0/120/FLUENT/flth.pdf

21 **Bakhtar, F., J. Young, A. White, and D. Simpson.** Classical nucleation theory and its application to condensing steam flow calculations. *Proc. Inst. Mech. Eng. Part C* , 2005, **219**, 1315-1333.

22 **Guha, A.** Transport and deposition of particles in turbulent and laminar flow. , 2008.

23 **Ryley, D. and J. Davies.** Effect of thermophoresis on fog droplet deposition on low pressure steam turbine guide blades. *Int J Heat Fluid Flow* , 1983, **4**, 161-167.

24 **White, A., J. Young, and P. Walters.** Experimental validation of condensing flow theory for a stationary cascade of steam turbine blades. *Philosophical Transactions of the Royal Society of London A: Mathematical, Physical and Engineering Sciences* , 1996, **354**, 59-88.

25 **Yau, K. and J. Young.** The deposition of fog droplets on steam turbine blades by turbulent diffusion. *Journal of turbomachinery* , 1987, **109**, 429-435.

26 **Young, J. and K. Yau.** The inertial deposition of fog droplets on steam turbine blades. *Journal of turbomachinery* , 1988, **110**, 155-162.

27 **Wilcox, David C.**, *Turbulence Modelling for CFD*, California, DCW Industries Inc., Nov 1994.

28 **ANSYS**, "Axial Turbine Equilibrium and Non- Equilibrium Steam Predictions", *ANSYS CFX Tutorials*, California, ANSYS Inc., Nov 2009, pg. 397-414.

29 **Knez , Saso.** Airfoil boundary layer, [Online]. May 2005,

Available: http://www-f1.ijs.si/~rudi/sola/drugi_seminar.pdf

30 **Peter, Hardi and Schlichenmaier,** Rolf. Introduction to Hydrodynamics

[Online]. Feb 2005,

Available: http://www3.kis.uni-freiburg.de/~schliche/lectures_files/hydro.pdf

31 **ANSYS**, ANSYS CFX-Solver Theory Guide [Online], Page-24, Available:

http://orange.engr.ucdavis.edu/Documentation12.1/121/CFX/xthry.pdf

32 **Patel, Y., G. Patel, and T. Turunen-Saaresti**. Influence of turbulence modelling on non-equilibrium condensing flows in nozzle and turbine cascade. *Int. J. Heat Mass Transfer*, 2015, **88**, 165-180.